Oceanologia, corrected, in press

https://doi.org/10.5697/OBOE5006

Statistical downscaling of global climate projections along the Egyptian Mediterranean coast

Mohamed ElBessa[1,2], Mohamed Shaltout*[,1]

Abstract
The climatic parameters (surface air temperature, surface relative humidity, surface wind regime, and mean sea level pressure) are important in addressing adaptation/mitigation to climatic changes. In particular, the recent and future of these climatic parameters along the Egyptian Mediterranean Coast (EMC) were analyzed based on hourly real observed data (2007–2020) and hourly reanalysis (ERA5) database (1979–2020) together with daily GFDL (global climate model) mini-ensemble mean (2006–2100). Recent climatic studies in the study area have not given enough attention to the downscaling approach, underscoring the need to set up a statistical downscaling technique to better understand the forces that govern climatic change. Here, we analyze the current climatic and future scenarios for the parameters studied in a three-step process. The first step is to study the current weather variabilities in the short term (14 years) using the real observed data. The second step is to describe the long-term (42 years) current weather variabilities over the studied stations using a reanalysis ERA5 database after bias removal by comparing with the observations. The third step is to statistically downscale the GFDL mini-ensemble, which means describing the future projection along the study area up to 2100. The statistical downscale technique is built on the developed bias correction statistical model by matching cumulative distribution functions (CDF) of the mini-ensemble mean and observations during the overlapped period (2007–2020).
The results show that ERA5 describes the efficiency of the weather characteristics of the five studied stations. This data, along with the EMC 2006–2020, displays a significant positive trend for surface air temperature and significant negative trends for surface wind speed, relative humidity, and sea level pressure. The GFDL mini-ensemble mean projection, up to 2100, has a significant bias with the studied weather parameters. This is partly due to the GFDL coarse resolution ($2^{\circ} \times 2.5^{\circ}$). After removing the bias, the statistically downscaled simulations from the GFDL mini ensemble mean show that the study area's climate will experience significant change, especially surface air temperature and relative humidity with a great range of uncertainties according to the scenario used and regional variations. Our results are the initial step in enhancing the understanding and development of statistical downscaling techniques to project future climate scenarios over EMC.

Keywords
Statistical downscaling; ERA5; GFDL; Air temperature; Relative humidity; Surface wind

[1] *Oceanography Department, Faculty of Science, Alexandria University, Alexandria 21526, Egypt*
[2] *College of Maritime Transport and Technology (CMTT), Arab Academy for Science, Technology and Maritime Transport (AASTMT), Abu-Qir, Alexandria, Egypt*
***Correspondence**: mohamed.shaltot@alexu.edu.eg

Received: 27 July 2023; **revised:** 23 June 2024; **accepted**: 22 August 2024

1. Introduction

The Egyptian Mediterranean coast (EMC), which extends from 27°E to 33°E (Figure 1), is considered an arid zone except for El Arish, which is considered a semi-arid zone (UNESCO, 1979). According to UNESCO (1979), the aridity index (the rate of annual precipitation/potential evapotranspiration) is between 0.03 and 0.2 for the arid zone and from 0.2 to 0.5 for the semi-arid zone. The study area provides a marketable resource for industrial activities, farming, fishing, tourism, oil, natural gas structures, and import and export activities. At the same time, the EMC has been confirmed as a climatic 'hot spot' region as it will experience significant changes in surface air temperature (positive trend) and rate of precipitation (negative trend), together with a slight decrease in sea level pressure at the end of the twenty-one centuries as stated by (Shaltout et al., 2013; IPCC, 2019; Tuel and El Tahir, 2020).

The study area suffers from severe climatic events, such as storms, as well as man-made pressures (such as random construction on the coasts), which makes this

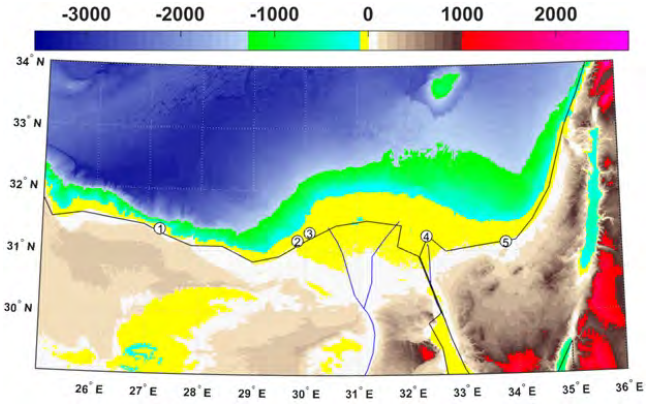

Figure 1. Bathymetric chart of the study area with the five considered weather observation stations: 1) Marsa Matrouh, 2) Ras El-Tin, 3) Abu Qir, 4) Port Said and 5) El Arish.

area highly vulnerable. Moreover, the EMC is also suffering from various problems, including dramatic population growth, land subsidence, saltwater intrusion, unplanned urbanization, high erosion rates, land use interference, soil salinization, ecosystem pollution, and degradation. Thus, EMC timely necessitates urgent needs to reconsider the current and future climate in order to switch the climate change threats into socioeconomic benefits (Agrawala et al., 2004).

In general, Egypt has four seasons: summer (June, July, and August), winter (December, January, and February), spring (March, April, and May), and autumn (September, October, and November). The climate of the winter season is cold, moist, and rainy. The summer season is hot, dry, and rainless, with clear skies. The main event in the spring season is the Khamasine Depression, and the climate in the autumn season is similar to that in spring, confirming another transitional season.

The EMC climate describes a seasonal variation. During the summer season, the Indian Summer Monsoon (ISM) and the Azores highly significantly control the EMC climate condition (Yadav, 2021). The Azores high, associated with a moderate climate, expands eastwards. At the same time, ISM, associated with thermal low, expands northwest. Thus, in the summer period when the ISM dominated over EMC, the extreme increase in temperature with high dry conditions is noteworthy. However, when the Azore's high dominates over the southeast Mediterranean, the temperature and dry conditions would be moderated.

During the winter season, the Mediterranean region is affected by the passage of occasional depressions that cross the region from west to East. This passage is accompanied by cold fronts sometimes and hot fronts at other times. Moreover, the Mediterranean Sea region is also affected by the presence of high-pressure systems that originated over Northern Europe and Asia, such as the Siberian winter high. After passing these occasional Depressions (if it is accompanied by cold fronts) over the Mediterranean Sea, the cold air coming from northern Europe (especially from Upper Siberia) rushes to the Mediterranean region, which leads to an increase in the degree of atmospheric stability. Thus, cumulus and cumulonimbus clouds can be formed, and precipitation is in the form of drizzles, snow, or hail. This depression may also be accompanied by thunderstorms, especially in areas where the fronts pass. Then, the air takes moderation until another depression comes, and so on. The weather in this season is often unstable, and the Mediterranean region is exposed to the invasion of continental/maritime polar air masses, especially in the northwest and the northeastern Mediterranean (Egyptian Naval Forces, 1962).

Occasionally, when the area of high pressure moves away from the United Kingdom to the Scandinavian countries, it is strengthening. The characteristics of the Blocking Anticyclone (omega block) system are remarkable. That prevents the normal Mediterranean Depression from passing from west to east. This blocking system guarantees calm and dry weather over the central-western part of Europe. In contrast, the central-eastern part of Europe and the eastern Mediterranean (including North Egypt) are characterized by cold air. As this configuration passes over the Mediterranean Sea, they gain water vapor from the Mediterranean Sea, which leads to an increase in the amount of rain in North Africa. While the presence of omega blocks coincides with the Siberian High, a decrease in temperatures and snowfall over North Asia and parts of Northeast Africa is noteworthy (Kautz et al., 2022).

Specifically, De Vries et al. (2013) showed that the Siberian High system significantly influences climate /weather fluctuations over the EMC and its surrounding continent. The Siberian High system, which is responsible for polar outbreaks over the Mediterranean Sea (Saaroni et al., 1996), tends to increase the likelihood of the rainy season developing, which, when combined with the Mediterranean low-pressure system, generates easterly storms over the EMC (Saaroni et al., 1998; Nastos and Zerefos, 2009). The southward movement of the Siberian High and Azores High over the Mediterranean Sea produces numerous advantages for precipitation and the development of extratropical storms (Haggag and El-Badry, 2013). Furthermore, when the Azores High (winter subtropical high-pressure systems) move southward, storm systems from the Atlantic Ocean tend to penetrate the Mediterranean Sea (Zerefos et al., 2011). Moreover, severe weather occurrences over EMC during the winter season are strongly linked to Mediterranean cyclones and very rarely occur under other conditions (Lionello et al., 2006).

Earlier studies on the following topics (surface air temperature, surface relative humidity, surface wind, and mean sea level pressure) are available, offering insightful information and fundamental understanding.

1.1 Surface air temperature (T2m)

Domroes and EL-Tantawi (2005) showed that in Marsa Matrouh the annual average T2m is 19.5°C with a warming trend of 0.18°C decade^{-1} using observation data from 1971 to 2000. At the same time, Shaltout et al. (2013) used the ERA-Interim dataset (1979–2010) to confirm that the annual average T2m ranges from 20–20.5°C with a warming trend of 0.4–0.5°C decade^{-1}. Over the period from 2007–2018, the monthly T2m ranges from 12.26°C (in January) to 27.93°C (in August) with a warming annual trend of 0.45°C decade^{-1} as stated by Tonbol et al. (2018). The hourly T2m over the period (2007–2016) reaches its minimum (maximum) value of 5.2°C (43.4°C), with an annual mean value of 20.6°C (El-Geziry et al., 2021).

In Alexandria, Domroes and EL-Tantawi (2005) used observation data from 1941–2000 to show that the annual average T2m is 20.3°C with a warming trend of 0.1°C decade^{-1}. While Shaltout et al. (2013) confirmed that the annual average T2m ranges from 20–20.5°C for the period 1979–2010 using the ERA-Interim dataset with a warming trend of 0.3–0.4°C decade^{-1}. Moreover, Alexandria T2m shows a significant monthly variation, reaching its maximum value in August (29°C) and its minimum value in January (14°C) with a warming trend of 0.2–0.5°C decade^{-1} as stated by Tonbol et al. (2018) using hourly observed data from 2007 to 2016. Mahfouz et al. (2020) showed that the hourly T2m over Alexandria has a range (7–41°C) for the period from 2007–2018 with a warming trend of 0.3–0.4°C decade^{-1}. Moreover, El-Geziry et al. (2021) stated that the hourly T2m ranged from 5.2 to 41.0°C for the period from 2007–2019, with an annual mean value of 21.9°C.

Port Said, Domroes, and EL-Tantawi (2005) used observational data from 1941–2000 to show that the annual average T2m is 20.3°C with a negative warming trend of −0.06°C decade^{-1}. From 1997 to 2009, the daily T2m has a range (of 7–34°C) with an annual average value of 21.2°C (Shaltout et al., 2013). Moreover, the mean monthly T2m (2007–2016) fluctuated between 13.61°C (in January 2012) and 29.50°C (in August 2015) stated by Tonbol et al. (2018). El-Geziry et al. (2021) confirmed that hourly (2007–2019) T2m reached its minimum (maximum) value of 1.0 (41.7) °C with 22.1°C as an annual mean value.

In El Arish, Shaltout et al. (2013) confirmed that the annual average T2m is 20.5°C for the period 1979–2010 using the ERA-Interim dataset with a warming trend of 0.5–0.6°C decade^{-1}. From 2007 to 2016, the hourly T2m shows a significant monthly variation, reaching its maximum value in August (29.3°C) and its minimum value in January (12°C) with a warming trend of 0.57°C decade^{-1} with an annual mean of 21.55°C as stated by Tonbol et al. (2018). Moreover, the hourly T2m (2007–2019) ranged from 2.0 to 45°C, with a mean value of 21.6°C (El-Geziry et al., 2021).

Alcamo et al. (2007) showed that T2m in the northern Mediterranean region under the A1B scenario is projected to experience a warming trend of 0.22–0.5°C decade^{-1} up to 2100. Alpert et al. (2008) reported a warming increase over the Eastern Mediterranean ranging from 4°C (A2 scenario) to 3°C decade^{-1} (B2 scenario) when comparing 2071–2100 and 1961–1990. The region of EMC will expect significant warming uncertainty ranging from 0.6–2.8°C by the end of the current century regarding the 1981–2010 average value as stated by Shaltout et al. (2013). Depending on the used scenario, the EMC will expect significant warming ranging from 0.6 to 2.6 °C. Generally, future warming signals over the study area are consistent features in the regional and global climate modeling through A1B and A2 scenarios (IPCC, 2014). Furthermore, Lelieveld et al. (2016) apply the ensemble results of CMIP5 models through RCP4.5 and RCP8.5 scenarios to confirm a significant warming trend, especially during summer over the MENA region (including the study area). Bucchignani et al. (2018) showed that T2m over the Middle East and North Africa domain under the RCP4.5 scenario will experience significant warming ranging from 2.5 to 4°C decade^{-1} by using the COSMO-CLM regional climate model.

1.2 Surface wind regime

Zecchetto and De Biasio (2007) show that the wind blowing from the Northwest describes the dominant wind field over the EMC. Moreover, along the EMC, the wind direction showed geographical variation, where the NW wind direction mostly dominates over the western part of the EMC and the WNW wind direction dominated over the eastern part of the EMC, as stated by Krichak et al. (2007). Furthermore, Elbessa et al. (2021) showed that the southerly wind direction did not significantly affect the study area except at El Arish station.

The wind direction over EMC showed a seasonal variation. However, the prevailing annual wind direction in front of Port Said and Alexandria was blowing from NW to N direction (Hamed, 1979, 1983; Meligy, 2000; Elsharkawy et al., 2016; Mahfouz et al., 2020). At Marsa Matrouh, the dominant wind was NW with a mean direction of 315° (El-Geziry et al., 2021). Over El Arish, the prevailing wind direction (2007–2018) was NNW (Elbessa et al., 2021). On the other hand, the wind speed showed a diurnal and seasonal variation (Sabra, 1979; Meligy, 2000). Over Alexandria, the maximum wind speed occurs from noontime to 3:00 PM, while the minimum speed occurs during the night from 9.00 PM to 6.00 AM. The maximum wind speed occurred during winter (interval of 9.1–11.4 m s^{-1} and > 11.9 m s^{-1}), while the minimum speed (3.8–5.4 m s^{-1}) occurred during summer (higher speed values in winter are due to the frequent occurrence of storms during winter). From another direction, the wind speed along the EMC shows a spatial variation, where El Arish (Port Said) has the smallest (largest) mean wind speed of 2.3 (4.9) m s^{-1}, as stated by Essa and Mubarak (2006).

In the winter along the EMC, a frequent short period

(2–4 days) with wind speed exceeding 17 m s^{-1} accompanied by severe weather conditions occurs between sunny spells or clear time intervals (Nawat). Following EAMS (2021), 21 frequent Nawat intervals have been identified over EMC, extending from the 17th of October to the 3rd of April. In general, all Nawat periods are associated with cold fronts accompanied by a sudden fluctuation of wind, usually to the N or NW. In the summertime, EMC is characterized by warm, good weather. The Asian anticyclone in summer extends westwards to Europe. Usually, it collides with an Eastern extension of the Azores anticyclone and cyclone over Syria, forcing the air to blow from north to northwest over the eastern Mediterranean region.

The study area has two important regional winds: the Scirocco (Khamasin) and Meltemi (Etesians) over EMC.

Scirocco (Khamasin) is a hot, dry desert wind blowing over North Africa. This Khamasin wind blows in front of the Mediterranean depressions passing from west to east along the Mediterranean Sea. When the center of these Mediterranean depressions travels from south to north, the accompanying wind is known as Scirocco. In this case, the Scirocco wind takes up water vapor from the Mediterranean Sea during its pass northward and turns into a warm and moist wind. Khamasin wind has various names according to the places they pass by; for example, in Libya, it is known by Ghibli, while over-Palestinian, Jordan, and Syria, it is known by Simoom (Egyptian Naval Forces, 1962).

The Meltemi (Etesians) is a katabatic, strong, dry wind blowing from the Black and Aegean Seas to the EMC region. Over EMC, the Meltemi wind blows from the Northwest direction, and thus, this wind moderates the high air temperature (Egyptian Naval Forces, 1962). According to Zecchetto and De Biasio (2007), the Meltemi wind is characterized by high steadiness and low wind variability.

1.3 Relative humidity (RH)

Sallam and Elsyed (2015) showed that the relative humidity over the Nile Delta coast from 2010 to 2013 fluctuated between 60% during April–June to 75% during January. Moreover, the monthly mean relative humidity over Alexandria (2007–2018) showed a significant monthly variation ranging from 77.6% during July/2009 to 57.3% during January/2008, with an annual average of 64.9% (Mahfouz et al., 2020). On the other hand, El-Geziry et al. (2021) stated that the mean relative humidity (2007–2019) was 70.2, 68.7, 73.0, 68.4, and 70.4% in Marsa Matrouh, Ras El Tin, Abu Qir, Port Said, and El Arish, respectively.

1.4 Sea level pressure (SLP)

According to Hamed (1983), the Egyptian Mediterranean coast shows significant SLP seasonal variation ranging from 1005.8–1013.9 hPa in summer to 1004.0–1025.3 hPa in winter. Moreover, Shaltout et al. (2013) showed that the ERA-Interim closely matches SLP observation. They also indicated that the Average Annual SLP (1978–2010) along the Egyptian Mediterranean coast showed a spatial variation ranging from 1013.12–1015.47 hPa, generally decreasing from west to east. The current SLP described a general negative trend of 0.305 hPa $decade^{-1}$, which is expected to continue up to 2100 with an uncertainty of 0–0.6 hPa $decade^{-1}$ (Shaltout et al., 2013). Specifically, the monthly SLP over Alexandria (2007–2018) showed significant monthly variations ranging from 1005.9 hPa during July/2012 to 1022.2 hPa during January/2007 (Mahfouz et al., 2020). They also showed that SLP over Alexandria has a significant annual variation, where the highest value was 1032.3 hPa during 2007, and the lowest value was 998.2 hPa in 2018(annual average SLP was 1013.5 hPa).

A summary of previous studies regarding T2m, RH, SLP, and surface wind fields, examining their average/trends across various cities along the EMC, are tabulated in Annex 1.

The current research used statistical downscaling techniques to project the future climate along EMC over Marsa Matrouh, Ras El-Tin, Abu Qir, Port Said, and El Arish. First, the observed data was used to describe the current short-term weather variabilities from 2007 to 2020. Secondly, the current research qualifies the use of ERA5 in capturing T2m, Rh, SLP, and surface wind fields. Third, 42 years (1979–2020) of ERA5 after bias removal are used to describe the current long-term climate variability. Finally, EMC's future climate is projected using a statistical downscaling technique through the four different CMIP5 scenarios. The materials and methods used are presented in section 2, the results and discussion in section 3, and the conclusions in section 4.

Despite the extensive previous studies to analyze the current status of atmospheric parameters along EMC, short-period studies seem to be a common problem in previous analyses of the recent atmospheric components. Thus, there is a need for more comprehensive and long-term studies to understand the recent changes to gain a better understanding of the recent changes in atmospheric parameters. On the other hand, there are limited climatic modeling studies along EMC, most of which depend on the analyses of regional climatic models. Analyzing statistical downscaling will support the previous modeling results and open a discussion for better study for future uncertainty. One approach to solve this problem involves using statistical downscaling that has emerged from analyzing 42 years of current atmospheric characteristics together with statically projecting these atmospheric characteristics up to 2100.

For our first goal, we focus on solving the previously mentioned problems. After solving these problems, we can show whether the EMC region warms more or less than neighboring regions. Thus, the current research findings will be of wide interest and will provide valuable data for policymakers and decision-makers in developing effective strategies and policies to adapt to changing climatic con-

ditions. Section 2 presents the materials and methods, while Section 3 displays the results. Section 4 presents the discussion and conclusions.

2. Material and methods

This paper used observation data to describe short-term atmospheric variability for T2m, RH, and SLP, as well as surface wind field components (eastward wind (U10), northward wind (V10), and SLP along EMC. Moreover, the long-term characteristics of the studied atmospheric parameters were analyzed using the ERA5 database after removing the bias. For the projection of future scenarios, statistical downscaling for the Geophysical Fluid Dynamics Laboratory (GFDL) mini-ensemble means was used to study the future projection over the study area (Figure 2).

2.1 Material

2.1.1 Observed data

Five Automated Weather Observing Systems (AWOS) along EMC were used to collect T2m, RH, SLP, U10, and V10 at Marsa Matrouh, Ras El-Tin, Abu Qir, Port Said, and El Arish, as seen in Figure 1 and Table 1. AWOS is installed and maintained according to WMO regulations. All readings are calibrated to WMO standard height (Table 1). The standard height is 0 m for SLP, 2 m for T2m and RH, and 10 m for U10 and V10. These five stations are well spatially distributed along EMC and extend from 2007 to 2020 on an hourly basis with 0% of missed data, showing the pioneers of the used data.

2.1.2 ERA5 database

Hourly data on T2m, RH, U10, V10, and SLP from 1979 to 2020 were obtained freely from the European Eyes on Earth (Copernicus) website (https://cds.climate.copernicus.eu/cdsapp#!/dataset/reanalysis-era5-single-levels?tab=form).

ERA5 data, which is distributed by the Copernicus Climate Change Service (C3S) and produced by the European Center for Medium-Range Weather Forecast (ECMWF), were intended to improve on the success of the earlier issues (e.g., ERA-Interim and ERA40) and improve atmospheric parameters (C3S, 2017; Hersbach and Coauthors, 2020), with a finer spatial grid of $0.25^\circ \times 0.25^\circ$ and temporal hourly resolution. After validation with observations, this data is used to analyze long-term trends of the stud-

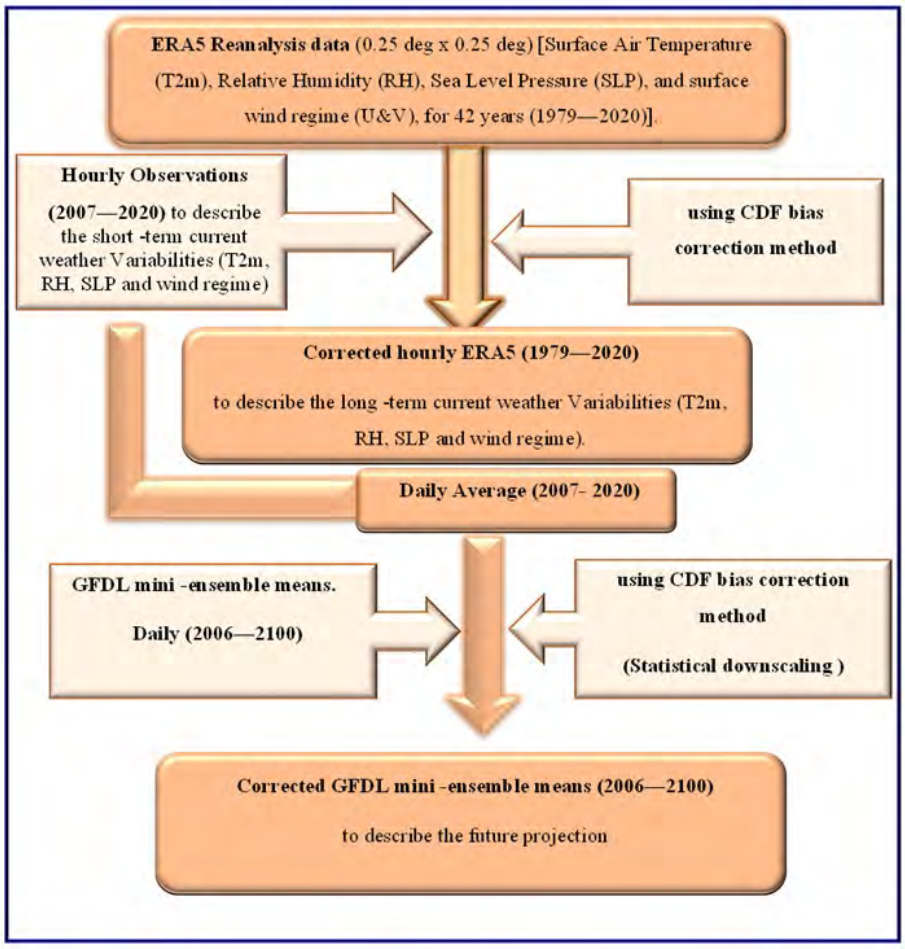

Figure 2. The theoretical framework (workflow).

Table 1. Elevations and positions of coastal Meteorological working stations (period of recorded data for all stations from 1st of January 2007 until the end of December 2020). The identification numbers (IN) 1 to 4 are also included in relation to Figure 1.

Station		Height above	Geographic position		International station
Names	IN	sea level [m]	Latitude	Longitude	number
Marsa Matrouh	1	20	31°21′34″	27°14′43″	62304
Ras El Tin	2	21.95	31°11′50″	29°51′49″	62317
Abu Qir	3	26.6	31°19′55″	30°5′6″	62320
Port Said	4	19.75	31°15′19″	32°18′17″	62334
El Arish	5	15	31°08′54″	33°49′27″	62331

ied atmospheric variables. Moreover, this data is used to statistically downscale global climate simulations over the five studied stations.

2.1.3 Modeled data (2006–2100)

The GFDL climate model simulation of surface air temperature (Tas), RH, SLP, U10, and V10 for the period 2006–2100 were extracted from three prototype models: GFDL-ESM2M (Dunne et al., 2012, 2013) GFDL-CM3 (Griffies et al., 2011), and GFDL-ESM2G (Dunne et al., 2012, 2013). These simulations are available on the GFDL website (ftp://nomads.gfdl.noaa.gov/CMIP5/output1/NOAA-GFDL) through four CMIP5 emission scenarios with a coarse grid resolution of $2^{\circ} \times 2.5^{\circ}$.

2.2 Methods

Observed data and the ERA5 database, together with the results from three different realizations based on the GFDL (Global Climate Model) configuration, were used to analyze recent and future variabilities for T2m, RH, 10 m height wind speed (WS_{10}), wind direction (WD_{10}), and SLP from 1979 to 2100.

Due to the absence of actual surface relative humidity (RH) data in the ERA5 (available only at the vertical level, not at the surface) and climate model output data sets, we calculated it based on T2m and surface dew point temperature (d2m) according to (Alduchov and Eskridge, 1996) as mentioned in Equation (1).

$$\mathrm{RH} = \frac{100 \times \exp\left(\frac{17.625 \times \mathrm{d2m(^{\circ}C)}}{243.04 + \mathrm{d2m(^{\circ}C)}}\right)}{\exp\left(\frac{17.625 \times \mathrm{T2m(^{\circ}C)}}{243.04 + \mathrm{T2m(^{\circ}C)}}\right)} \tag{1}$$

2.2.1 Observation

The observed T2m, RH, WS_{10}, and SLP data were subjected to statistical analyses (mean, standard deviation, minimum, and maximum) to investigate its temporal variation on hourly, daily, monthly, and annual bases. In addition, the wind rose is used similarly to describe temporal variation in WD_{10}.

2.2.2 The CDF approach

In accordance with Vigaud et al. (2013), the CDF approach can be used as follows: For weather station, let F_h represent the CDF of observed local data from 2007 to 2020; E_h represent the CDF of ERA5 outputs bi-linearly interpolated at the exact station location; G_h represents the CDF of GFDL mini-ensemble mean bi-linearly interpolated at the same station location for the same period; and F_f and G_f represent their corresponding values for the future (2020–2100) GFDL mini-ensemble mean outputs and observed outputs, respectively. Based on the presumption that a transformation T exists, transforming the CDF of ERA5/GFDL mini-ensemble mean variable (predictor) into the CDF representing the observation (predictand) at the specified weather station, the bias correction technique is implemented T: [0, 1] → [0, 1]

$$T(E_h(x)) = (F_h(x)) \tag{2}$$

Replacing x by $E_h^{-1}(u)$ in Equation (2) with $u \in [0,1]$ allows the following definition for the transform T:

$$T(u) = F_h(E_h^{-1}(u)) \tag{3}$$

Similarly,

$$T(u) = F_h(G_h^{-1}(u)) \tag{4}$$

Assuming that this later relationship remains valid in the future (i.e. $F_f = T\ (G_f)$), the researched CDF is given by:

$$F_f(x) = F_h\left(G_h^{-1}\left(G_f(x)\right)\right) \tag{5}$$

2.2.3 ERA5

Direct comparisons of the hourly-observed data and ERA5 are used to test the efficiency of ERA5 over the studied five stations. Moreover, the f- and t-tests are used to examine whether ERA5 and the observations display equal means and variances (come from the same population) or not at a 95% significance level. In addition, ERA5 databases are subjected to CDF bias correction between ERA5 and observation over 2007–2018 (calibration period). The years from 2019 to 2020 are used for the validation processes between ERA5 and observation.

The present strategy for bias correction is to match the cumulative distribution function (CDF) of the observations to the CDF of the ERA5 database at the station level (Equation (3)). The spatial mismatch between the point observation and the ERA5 grid cell is challenging in this bias correction. Only stationary points were analyzed in the current study. Therefore, our strategy is not affected by this challenge. Moreover, calibration and validation techniques are used to test the efficiency of ERA5 and to describe the weather characteristics of the five stations studied. Many researchers have used this strategy. Anagnostou et al. (1999) used the CDF strategy to adjust the satellite microwave for monthly rainfall estimates statistically. Furthermore, Wood et al. (2002) used the CDF technique for long-range hydrologic forecasting. Reichle and Koster (2004) used this strategy to match the CDF between satellite retrievals and model soil moisture. Finally, Bawadekji et al. (2022) used this strategy to match the CDF between observed and ERA5 atmospheric parameters along the Red Sea Saudi Arabia coast.

A boxplot analysis is used to visually show the distribution of C_ERA5 (ERA5 after bias removal) by presenting the data quartiles and averages on a monthly basis. Box plots display 1) the minimum value, 2) the lower quartile, 3) the median, 4) the upper quartile, and 5) the maximum value, as stated by Williamson et al. (1989).

A linear trend analysis, based on the ERA5 after correction (hereafter, C_ERA5) from 1979 to 2020, is used to characterize the current long-term climate along EMC over the studied five stations. Moreover, the non-parametric Mann-Kendall test (Mann, 1945; Kendall, 1975) is used to detect monotonic trends in C_ERA5 to examine whether C_ERA5 follows a significant (monotonic) trend or not. The limitations of the Mann-Kendall test are frequently associated with serial correlation data. The term "serial correlation" refers to the relationship between two variables with various lag periods. Each observation is independent of the other if the serial correlation of a variable is 0. If the serial correlations tend to be one, the observations are serially correlated, and the Mann-Kendall test will not identify monotonic trends (Wang et al., 2020). A trend-free prewhitening technique was used to avoid this limitation in the studied atmospheric parameters (Ahmed et al., 2015).

In addition, the studied atmospheric parameters are analyzed to establish the dates of the historically most extreme events (date of the maximum/minimum values) based on the C_ERA5 hourly data. The surface relative humidity value by itself is a relatively useless term without the accompanying temperature value. Thus, the temperature humidity index (THI; Liljegren et al., 2008) will be used instead of relative humidity to determine extreme heat stress events.

$$\mathbf{THI} = \mathrm{T2m} - 0.55(1 - [\mathrm{RH}/100])(\mathrm{T2m} - 14.44) \quad (6)$$

in which T2m is in °C and RH in %.

The levels of risks corresponding to given heat stress were classified according to the THI (°C) values and are reported by Liljegren et al. (2008) as follows:

(i) $\mathbf{THI}\,(^{\circ}\mathrm{C}) < 27$: Safe.

(ii) $27 \leq \mathbf{THI}\,(^{\circ}\mathrm{C}) < 32$: Heat fatigue is possible with prolonged exposure and activity.

(iii) $32 \leq \mathbf{THI}\,(^{\circ}\mathrm{C}) < 41$: Sunstroke and heat exhaustion are possible with prolonged exposure and activity.

(iv) $41 \leq \mathbf{THI}\,(^{\circ}\mathrm{C}) < 54$: Sunstroke and heat cramps are possible.

(v) $\mathbf{THI}\,(^{\circ}\mathrm{C}) \geq 54$: Sunstroke, heat stroke, heat confusion, or delirium are possible.

Furthermore, by splitting the complete range of the hourly data into a limited number of intervals (bins equal to 1°C for T2m and THI, 0.5 m s^{-1} for WS_{10}, and 0.5 hPa for SLP), the histogram is utilized to depict the probability density of hourly data values. The horizontal axis indicates the probable range of daily data values in the current study, while the vertical axis reflects the frequency of occurrence [%].

2.2.4 Statistical downscaling for future projection

Often, before conducting any research on the effects of climate change, climatic simulations must be adjusted. Specifically, the output of Global Climate Models (GCMs) might be affected due to systemic biases inherent in the model. Regular temperature deviation is one of the common problems. These biases result from factors like low geographical resolution, oversimplified thermodynamic processes, and insufficient understanding of the Earth's climate system. According to the Copernicus website (https://climate.copernicus.eu/sites/default/files/2021-01/infosheet7.pdf; accessed on June 3rd 2024), using uncorrected model outputs in impact assessments can result in inflated forecasts. Therefore, considering the variations in the mean and variability between GCM and observations during a reference period, the Bias Correction technique is employed to correct the projected raw GCM output (Vaittinada Ayar, 2021).

The results of the three GFDL realizations are averaged to calculate the GFDL mini-ensemble mean from 2006 to 2100. Then, the CDF of daily observation is matched with the CDF of the daily GFDL mini-ensemble mean under a control period (2007–2020) to describe a simple statistical model for bias removal from GFDL mini-ensemble mean simulation (Equation (4)). This statistical model is used to statistically downscale the studied atmospheric four parameters up to 2100 under different future RCPs scenarios. The statistically downscaled GFDL mini-ensemble mean simulations (hereafter, S_D_GFDL mini-ensemble mean) were used to calculate atmospheric future projection with better accuracy and validity along EMC (Equation (5)). The

future projections for the studied atmospheric parameters under the four RCPs scenarios were calculated using the 30-year running average.

According to Moss et al. (2010), four potential climate scenarios by 2100 are included in the Representative Concentration Pathways (RCPs). RCP2.6, RCP4.5, RCP6.0, and RCP8.5 are among them; the number indicates the extra radiative forcing (watts/square meter) in 2100 compared to preindustrial times. A scenario with global warming considerably below 2°C relative to pre-industrial temperatures is described by RCP2.6. Another depicts a bleak future where there is no climate mitigation strategy and a heavy reliance on fossil fuels, which will result in a temperature of almost 5°C by the end of the century, as described by RCP8.5.

Hausfather and Peters (2020) claim that the world envisioned in RCP8.5 is one that gets more improbable with every passing year. They also claim that current emissions are in line with median scenarios. However, the current research only used the RCP8.5 scenario to investigate an improbable, high-risk future similar to Riahi et al. (2010).

3. Results

3.1 Observed data

3.1.1 Monthly time series

Monthly average time series for T2m, RH, WS_{10}, and SLP based on hourly Observed data (2007–2020) over Marsa Matrouh, Ras El-Tin, Abu Qir, Port Said, and El Arish were shown in Figure 3. Moreover, the wind rose as a graphic tool is used to give a clear image of how WD_{10} changed monthly (Annex 2).

Marsa Matrouh

T2m data illustrated that January 2012 (12.3°C) was the coldest month, while August 2015 was the warmest month (27.9°C), as shown in Figure 3A. Likewise, RH data shows that the maximum monthly RH (79.6%) occurred during July 2013, whereas February 2020 had the lowest one (53.3%), as illustrated in Figure 3B. Additionally, WS_{10} data shows that January 2019 describes the windiest month (7.4 m s^{-1}), while November 2010 describes the calmest month (2.6 m s^{-1}), as noticed in Figure 3C. Normally, SLP data discloses that January 2012 describes the minimum monthly SLP (1008.6 hPa), while January 2017 depicts the highest one (1023.0 hPa), as seen in Figure 3D.

Abu Qir

T2m data shows that January 2012 (14.0°C) is the coldest month, while August 2015 (28.5°C) is the warmest month, as shown in Figure 3A. The RH data also confirmed that July 2020 (81.7%) had the maximum monthly RH mean, while February 2010 (63.8%) had the lowest rate, as illustrated in Figure 3B. Figure 3B. Likewise, WS_{10} data reveals that January 2020 (8.4 m s^{-1}) describes the windiest month, while August 2017 (3.9 m s^{-1}) describes the calmest month, as noticed in Figure 3C. Additionally, SLP data reveals that December 2015 (1022.0 hPa) describes the maximum monthly SLP, while July 2012 (1006.6 hPa) describes the lowest one, as shown in Figure 3D.

Ras El-Tin

T2m data reveals that January/2019 (14.2°C) is the coldest month, while August 2015 is the warmest month (29.1°C), as shown in Figure 3A. Likewise, RH data shows that July 2010 had the maximum monthly RH mean (77.6%), while January 2008 had the lowest one (57.3%), as seen in Figure 3B. In addition, WS_{10} data shows that January 2020 describes the windiest month (8.3 m s^{-1}), while August 2007 describes the calmest month (2.8 m s^{-1}), as illustrated in Figure 3C. Generally, SLP data reveals that January 2007 describes the maximum monthly SLP (1022.2 hPa), while July 2012 describes the lowest one (1005.9 hPa), as noticed in Figure 3D.

Port Said

T2m data illustrated that January 2015 (13.6°C) is the coldest month, while August 2015 is the warmest month (29.5°C), as shown in Figure 3A. Similarly, RH data showed that August 2010 had the maximum monthly RH mean (74.4%), while November 2016 had the lowest one (60.2%), as shown in Figure 3B. In addition, WS_{10} data reveals that March 2020 is the windiest month (6.2 m s^{-1}), while December 2020 is the calmest month (3.2 m s^{-1}), as noticed in Figure 3C. Additionally, SLP data reveals that January 2007 describes the maximum monthly SLP (1023.1 hPa), while July 2012 describes the lowest one (1007.2 hPa), as shown in Figure 3D.

El Arish

T2m data showed that January 2008 (12.0°C) was the coldest month, while August 2015 (29.3°C) was the warmest month. Likewise, RH data confirmed that July 2007 (78.7%) had the maximum monthly RH mean, while January 2019 (59.9%) had the lowest one. Furthermore, WS_{10} data reveals that March 2007 (5.8 m s^{-1}) describes the windiest month, while November 2018 (2.8 m s^{-1}) describes the calmest month. Generally, SLP data showed that December 2015 (1022.2 hPa) describes the maximum monthly SLP, while August 2008 (1005.4 hPa) describes the lowest one.

In general, the annual average T2m along the EMC reaches its maximum value over Port Said (22.0°C) and its minimum value over Marsa Matrouh (20.5°C), following the pattern that the annual average T2m increases gradually from Marsa Matrouh to Port Said then decreases again toward El Arish.

On the other hand, the annual average RH over Ras El Tin and Port Said showed a similar value (RH $= 68.5\%$), partially due to the similarity of land use around the two

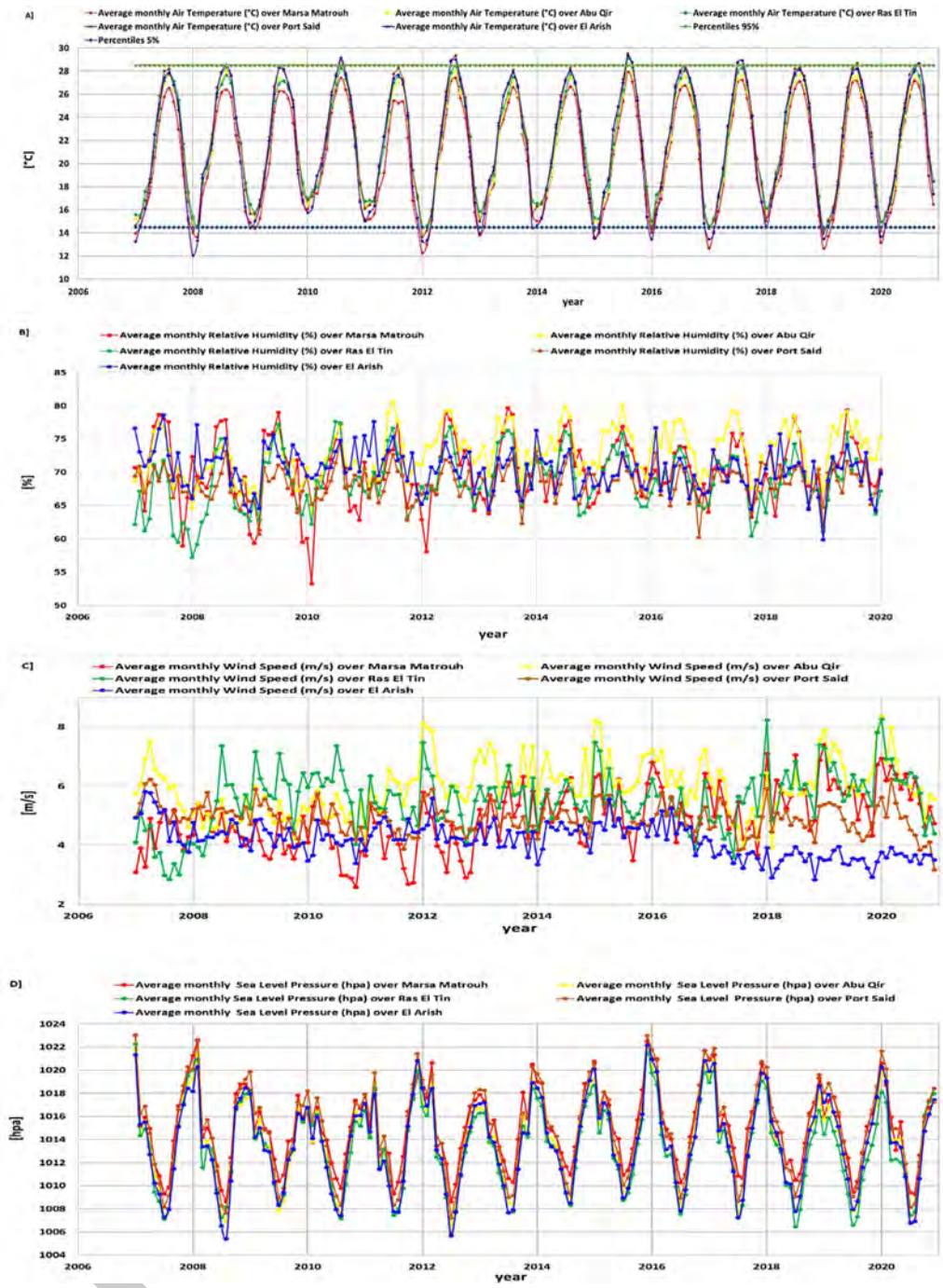

Figure 3. Monthly average time series for the parameters understudy is based on hourly observed data (2007–2020) over Marsa Matrouh, Abu Qir, Ras El Tin, Port Said, and El Arish.

stations (sea from the Northern directions and populated area from the Southern side). Likewise, the annual average of RH over El Arish and Marsa Matrouh is similar (RH $= 70.4\%$), partially due to the similar nature of these two stations (sea from the Northern direction and desert from the Southern part). The maximum annual average of RH along the five stations occurred over Abu Qir (RH $= 73.2\%$), partially attributed to the location of the Abu Qir station, which is located at the end of the pier that extends into the sea.

Regarding the WS_{10} horizontal distribution, the annual average WS_{10}, along with the EMC, reaches its maximum value over Abu Qir (5.9 m s^{-1}) and Ras El-Tin (5.5 m s^{-1}). The minimum annual average WS_{10} value (4.2 m s^{-1}) was recorded across El Arish stations.

Regarding SLP horizontal distribution, the annual av-

Table 2. Annual, monthly, and hourly characteristics for the parameters understudy based on hourly observed data (2007–2020) over Marsa Matrouh, Abu Qir, Ras El Tin, Port Said, and El Arish.

Variables		Marsa Matrouh		Abu Qir		Ras El Tin		Port Said		El Arish	
		Max	Min	Max	Min	Max	Min	Max	Min	Max	Min
Surface air temperature (T2M, °C)	Annual	2010 (21.56°C)	2011 (19.64°C)	2010 (22.26°C)	2011 (21.17°C)	2018 (22.38°C)	2011 (21.49°C)	2010 (22.90°C)	2007 (21.68°C)	2010 (22.31°C)	2007 (21°C)
	Monthly	August 26.83°C	January 14.03°C	August 27.64°C	January 15.31°C	August 27.99°C	January 15.59°C	August 28.51°C	January 14.86°C	August 28.36°C	January 13.88°C
	Hourly	23.21°C at 13.00	17.81°C at 05.00	23.03°C at 14.00	20.02°C at 04.00	23.63°C at 13.00	20.24°C at 04.00	24.62°C at 13.00	19.86°C at 04.00	25.11°C at 12.00	18.10°C at 05.00
Relative humidity (RH, %)	Annual	2020 72.08%	2010 67.14%	2020 75.80%	2008 70.05%	2013 70.60%	2007 64.86%	2020 69.59%	2009 67.46%	2007 72.57%	2019 69.24%
	Monthly	July 76.58%	February 66.32%	July 78.09%	November 69.98%	July 75.02%	December 65.23%	July 71.23%	November 66.49%	July 73.02%	December 67.48%
	Hourly	77.86% at 04.00	61.84% at 13.00	79.40% at 04.00	67.16% at 14.00	74.66% at 04.00	62.58% at 13.00	78.08% at 04.00	57.88% at 12.00	80.27% at 04.00	58.46% at 11.00
Surface wind speed (WS_{10}, $m\,s^{-1}$)	Annual	2020 (5.86 $m\,s^{-1}$)	2011 (3.98 $m\,s^{-1}$)	2019 (6.65 $m\,s^{-1}$)	2008 (4.92 $m\,s^{-1}$)	2019 (6.28 $m\,s^{-1}$)	2007 (3.81 $m\,s^{-1}$)	2007 (5.31 $m\,s^{-1}$)	2011 (4.59 $m\,s^{-1}$)	2007 (4.84 $m\,s^{-1}$)	2019 (3.47 $m\,s^{-1}$)
	Monthly	March 5.41 $m\,s^{-1}$	November 4.02 $m\,s^{-1}$	March 6.53 $m\,s^{-1}$	August 5.48 $m\,s^{-1}$	July 6.15 $m\,s^{-1}$	November 4.92 $m\,s^{-1}$	March 5.60 $m\,s^{-1}$	November 4.50 $m\,s^{-1}$	March 4.54 $m\,s^{-1}$	November 3.82 $m\,s^{-1}$
	Hourly	6.51 $m\,s^{-1}$ at 13.00	3.73 $m\,s^{-1}$ at 01.00	6.63 $m\,s^{-1}$ at 16.00	5.35 $m\,s^{-1}$ at 05.00	6.33 $m\,s^{-1}$ at 14.00	4.94 $m\,s^{-1}$ at 04.00	6.18 $m\,s^{-1}$ at 14.00	3.70 $m\,s^{-1}$ at 04.00	6.07 $m\,s^{-1}$ at 14.00	3.05 $m\,s^{-1}$ at 02.00
Mean sea level pressure (SLP, hPa)	Annual	2015 1016.06 hPa	2010 1014.13 hPa	2015 1014.81 hPa	2010 1012.99 hPa	2017 1014.16 hPa	2019 1012.01 hPa	2017 1015.86 hPa	2010 1014.09 hPa	2015 1014.72 hPa	2010 1012.86 hPa
	Monthly	January 1019.32 hPa	July 1010.1 hPa	January 1018.38 hPa	July 1007.99 hPa	January 1018.06 hPa	July 1007.50 hPa	January 1019.96 hPa	July 1008.77 hPa	January 1018.78 hPa	July 1007.65 hPa
	Hourly	1015.57 hPa at 10.00	1014.65 hPa at 04.00	1014.33 hPa at 10.00	1013.49 hPa at 04.00	1013.96 hPa at 10.00	1012.87 hPa at 04.00	1015.59 hPa at 09.00	1014.25 hPa at 15.00	1014.49 hPa at 09.00	1012.99 hPa at 15.00

erage SLP along the EMC reaches its maximum value over Marsa Matrouh and Port Said (1015 hPa) and its minimum value (1013.6 hPa) over Abu Qir, Ras El-Tin, and El Arish stations. This refers to the complexity of the SLP system along the EMC, where the maximum value was recorded in the western section (Marsa Matrouh station), followed by a gradual decrease until Abu Qir, then a rise until Port Said, then a decrease again until El Arish.

3.1.2 Annual, monthly, and hourly cycle

Over Marsa Matrouh, Abu Qir, Port Said, and El Arish stations, the hottest year is 2010, while over Ras El Tin, the hottest year is 2018. Likewise, the coldest year is 2011 (2007) over the Western (Eastern) side of EMC. According to RH analysis, the highest annual average RH along EMC is 2020 over Marsa Matrouh, Abu Qir, and Port Said stations, 2013 over Ras El Tin, and 2007 over El Arish. On the other hand, the lowest annual average RH along EMC occurred during 2010, 2008, 2007, 2009, and 2019 over Marsa Matrouh, Abu Qir, Ras El Tin, Port Said, and El Arish stations, respectively. Furthermore, the maximum annual average of WS_{10} along EMC occurred during 2020 over Marsa Matrouh, 2019 over Abu Qir and Ras El Tin, and 2007 over Port Said and El Arish, partially dividing the study area into three patterns. The minimum annual average of WS_{10} occurred in 2011 over Marsa Matrouh and Port and occurred in 2008, 2007, and 2019 over Abu Qir, Ras El Tin, and El Arish stations, respectively. Finally, the maximum annual average of SLP along EMC shows a similar pattern over Marsa Matrouh, Abu Qir, and El Arish, where the maximum (minimum) annual values occurred during 2015 (2010). Over Ras El Tin and Port said, the maximum annual SLP average occurred during 2017, while the minimum values occurred during 2019 and 2010, respectively, as seen in Table 2.

For the annual cycle (climate monthly average) as described in Table 2 and Figure 4, the annual T2m cycle has a maximum value in August and a minimum value in January, along with the five stations studied. The amplitude of the T2m annual cycle describes a variation from 12.3°C over the Abu Qir station to 14.5°C over the El Arish station. The annual RH cycle had a maximum value in July, along with the five stations studied. Meanwhile, the minimum value occurred in February over Marsa Matrouh, in November over Abu Qir, Port Said, and in December over Ras El Tin and El Arish. The amplitude of the RH annual cycle describes a variation from 4.74% over the Port Said station to 10.26% over the Marsa Matrouh station. According to WS_{10} analysis, its annual cycle has a maximum value in March over Marsa Matrouh, Abu Qir, Port Said, and El Arish stations and in July over Ras El Tin. Likewise, the minimum value happened in November over Marsa Matrouh, Ras El Tin, Port Said, and El Arish stations and in August over Abu Qir. The amplitude of the WS_{10} annual cycle describes a variation from 0.72 m s^{-1} over El Arish to 1.39 m s^{-1} over Marsa Matrouh station. Finally, the annual SLP cycle has a maximum (minimum) value that occurred during January (July) along with the studied five stations. However, the amplitude of the SLP annual cycle describes a variation

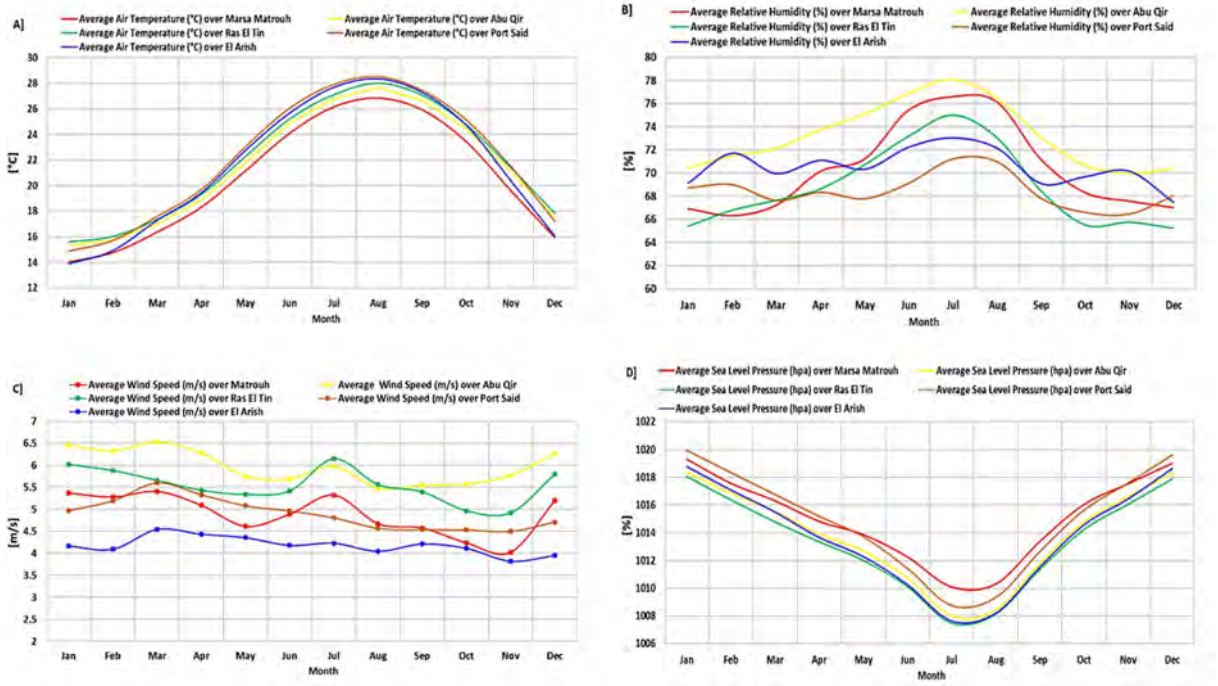

Figure 4. Observed short-term monthly means (annual cycle) for the parameters understudy based on hourly observed data (2007–2020).

from 9.22 hPa over Marsa Matrouh to 11.19 hPa over Port Said station.

The amplitude of the daily T2m cycle over El Arish (7.01°C) is much higher than that over Marsa Matrouh (5.4°C), Abu Qir (3.1°C), Ras El Tin (3.39°C), and Port Said (4.76°C). Similarly, the amplitude of the RH daily cycle over El Arish (21.81%) is much higher than that over Marsa Matrouh (16.02%), Abu Qir (16.02%), Ras El Tin (12.08%), and Port Said (20.20%). In the same way, the amplitude of the WS_{10} daily cycle reaches its maximum value (3.02 m s^{-1}) over El Arish and its minimum value (1.28 m s^{-1}) over Abu Qir. Habitually, the amplitude of the SLP daily cycle showed its maximum values (1.5–1.34 hPa) over the Eastern part of the study area (El Arish and Port Said) while showed its minimum values (0.84–0.92 hPa) over the Eastern part of the study area (Abu Qir and Marsa Matrouh) as shown in Table 2 illustrated in Figure 5.

In detail, the T2m showed a diurnal cycle along EMC, whereas the minimum value occurred between 04:00–05:00, and the maximum value occurred between 12:00–13:00. T2m showed two patterns regarding the daily range, where the daily range showed its maximum value over cities with desert nature (Marsa Matrouh and El Arish). Over the cities with agricultural nature (Abu Qir, Ras El Tin, and Port Said), the daily T2m range showed its minimum value (Figure 5).

Similarly, the RH showed a diurnal cycle along EMC, which reached the maximum value at 4:00, and the minimum value occurred between 11:00–14:00. The time associated with the lowest values of RH changed smoothly from the Eastern side of the study area (11:00) to the Western side of the study area (14:00).

The WS_{10} showed a diurnal cycle along EMC, whereas the maximum (minimum) value occurred between 13.00–15.00 (01:00–05:00). The WS_{10} daily range describes a variety of values ranging from 1.3 m s^{-1} over Abu Qir to 3.0 m s^{-1} over El Arish.

The SLP showed a semi-diurnal cycle along EMC which reached the maximum (minimum) value between 9–10 and between 21–22 (occurred between 3–4 and between 15–16). The observed short-term hourly means of SLP showed two patterns were noteworthy: one for the West (Marsa Matrouh, Abu Qir, and Ras El Tin) and the other for the East (Port Said and El Arish), which attributed to the pathway of the depressions from western point to Northeastern towards Cyprus (called Cyprus Depressions).

The wind direction at 10 m height (WD_{10})

The prevailing observed wind direction is coming from the NNW direction at Marsa Matrouh and Ras El Tin; however, it is coming from the N direction at Abu Qir, Port Said, and El Arish stations, as shown in Figure A2-1. It's clear that ERA5 represents the observed wind direction well, especially at Marsa Matrouh. Although the 45° (22.5°) clockwise deviations from Observed and ERA5 results at Abu Qir (El Arish).

It is noted in El Arish that the southern winds are indicated by the observed data, while the ERA5 data failed to clarify these southern winds. Thus, an intensive analysis was conducted in El Arish to monitor this Southern wind. These southern winds are concentrated from November to February, as seen in Annex 2 (Figure A2-6), and from 00:00–08:00 (data not shown) at El Arish with an average wind speed of 2.90 ± 1.03. This may be explained by the effect of the land breeze, which dominates during the night and winter. In addition, the nature of the El Arish area has an average elevation between 400 to 500 meters towards the south, which leads to enhancing the effect of the katabatic wind. In the other four cities, the southern wind was not adequately monitored, which attracted our attention, and we will address this in our next research.

In Marsa Matrouh (Figure A2-2), the Western wind is predominant from December to February, while the NW-NNW wind is predominant from March to September. During October and November, the Northern wind dominated. At Abu Qir (Figure A2-3) and Ras El Tin (Figure A2-4), the Northern wind dominated from September to December, while the Western wind prevailed during January and February. In addition, the North's winds prevail again from March to May. From June to August, the NW wind prevails.

The prevailing winds at Port Said (Figure A2-5)) fluctuated between northern and western winds from December to February. For the rest of the year, the Northern wind dominated.

In Arish (Figure A2-6), Southern winds prevail from November to January. During the following month (February), the prevailing winds fluctuated between Northern and Southern winds. The prevailing winds blow from the north during the other eight months (March to October).

3.2 ERA5 reanalysis data

3.2.1 ERA5 calibration

To evaluate the convenience of using ERA5 in describing the atmospheric parameters over Marsa Matrouh, Ras El Tin, Abu Qir, Port Said, and El Arish, a comparison was carried out between ERA5 datasets and observation data covering the observation period from 2007 to 2018 (Table 3 and Figures A2-2–A2-6).

In general, the ERA5 reanalysis data closely matched the observations of the five studied stations. ERA5 lower estimate of T2m observation at Abu Qir, Ras El-Tin, Port Said, and El Arish by 0.4°C, 0.7°C, 0.5°C, and 0.4°C respectively. However, the ERA5 overestimates T2m at Marsa Matrouh by 0.1°C. Furthermore, the ERA5 lower estimate RH observation at Marsa Matrouh by 3.6% and Abu Qir by 1.8%. Meanwhile, ERA5 overestimated RH at Ras El-Tin, Port Said, and El Arish by 3.5%, 1.1%, and 0.6%, respectively. Regarding the WS_{10}, ERA5 underestimates WS_{10} at Marsa Matrouh, Abu Qir, Ras El-Tin, and Port Said by

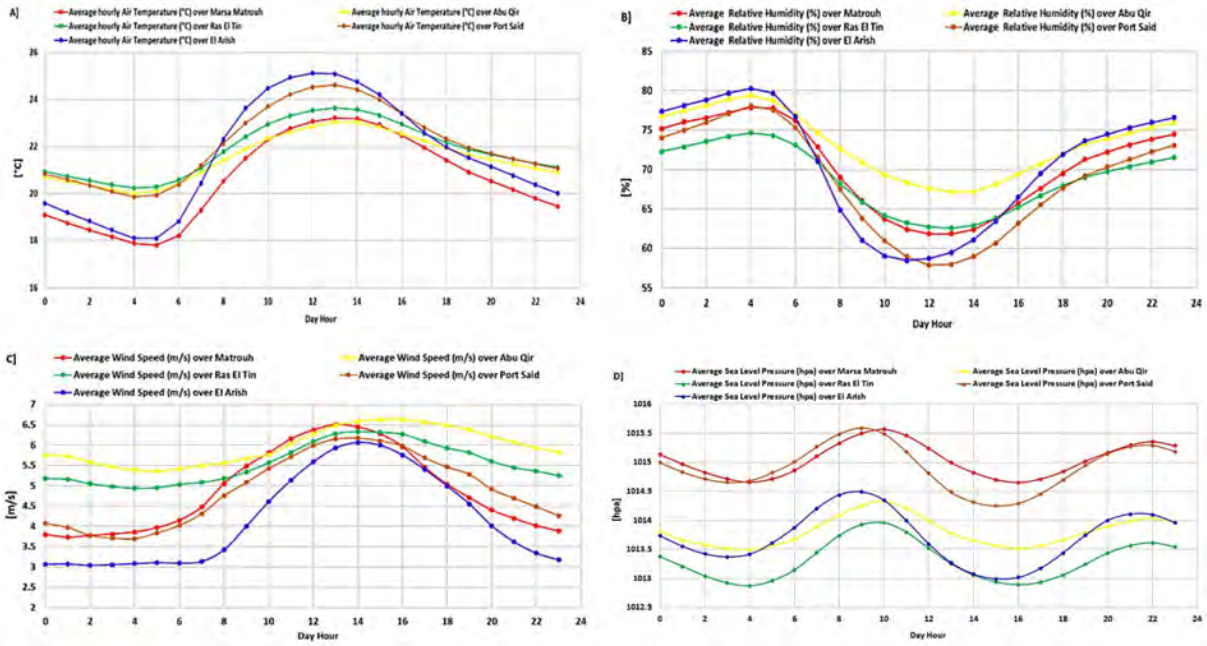

Figure 5. Observed short-term hourly means (daily cycle) for the parameters understudy based on hourly observed data (2007–2020).

0.1 m s^{-1}, 1.5 m s^{-1}, 0.3 m s^{-1}, and 0.2 m s^{-1}, respectively. ERA5 showed an identical average value to the observed WS_{10} in El Arish. Moreover, the ERA5 datasets lower the estimated SLP observations at Marsa Matrouh, Port Said, and El Arish by 1.1 hPa,1.3 hPa, and 0.2 hPa, respectively. In the other stations, ERA5 overestimated SLP at Abu Qir by 0.4 hPa and Ras El-Tin by 1 hPa, as shown in Table 3.

At a 99% significance level, statistical tests (t- and f-tests) indicated that ERA5 and observed datasets of T2m, RH, WS_{10}, and SLP values come from two equal distributions of mean and variance. Despite smoothing the processing of ERA5, which decreases the agreement between ERA5 and observed wind direction both datasets are in good agreement (Figures A2-2–A2-6).

3.2.2 ERA5 bias correction

To remove the ERA5 bias, CDF bias correction is applied to match the CDF of the ERA5 to the CDF of the observation from 2007 to 2018, as seen in Annex 3 (Figure A3-1). This technique preserves the nature of the data by adjusting the bias to zero, and the correlation value can be changed due to non-linear quantile bias correction. This strategy was applied for the long-term ERA5 database to calculate the corrected ERA5 reanalysis data (C_ERA5) over the five studied stations. Figure A3-1 proves the current results that ERA5 reanalysis data more reasonably simulates the current atmospheric parameters over all stations as the three curves of observations, ERA5 and C_ERA5, are so close. Moreover, we used the validation strategy to check the efficiency of using the C_ERA5 over the studied stations (as seen in section 3.2.3).

3.2.3 ERA5 validation

In this section, the validation is used to evaluate whether a calculated statistical model during the calibration period is appropriate or not. Table 4 shows the comparison between ERA5 and C_ERA5 in describing the weather characteristics over the studied five stations. It's evident that the C_ERA5 showed a lower bias with the observation than ERA5 did. However, the correlation between the C_ERA5 and observation showed a similar value as ERA5 did. Therefore, using C_ERA5 is useful and valid for describing the long-term current weather characteristics and gives a better weather description of the studied stations.

3.2.4 C_ERA5 statistical analyses

Boxplot analysis

All the studied meteorological parameters exhibit a significant monthly variation. The 75th percentile of T2m occurred in August over all the studied stations. While the 75th percentile of WS_{10} and SLP occurred through December and January, as seen in Figures 6, 7 and 8, along the Egyptian Mediterranean Coast. On the other hand, the 75th percentile of RH occurred in hot months (June, July, and August), where the 75th percentile of RH is so close during these months at the studied stations as illustrated in Figure 9. Moreover, the outliers' values for T2m and WS_{10} are mostly above the upper quartile values, while the outliers' values for RH are mostly below the lower quartile values. In the same context, the outliers' values for SLP are distributed above the upper quartile and below the lower

Table 3. Comparison analysis between observed and ERA5 (for the calibration period; 2007–2018) weather variables over Marsa Matrouh, Abu Qir, Ras El Tin, Port Said, and El Arish: n = number of observations, R = correlation coefficient.

Variables			n	R [%]	Minimum	Maximum	Annual mean ± standard deviation of the annual cycle
Surface air temperature (T2M, °C)	Marsa Matrouh	Observed	105192	95.8	5.2	43.4	20.6 ± 5.3
		ERA5			5.1	44.2	20.7 ± 5.9
	Abu Qir	Observed	105096	97.3	7.4	38	21.51 ± 4.8
		ERA5			7.0	36.7	21.07 ± 4.7
	Ras El Tin	Observed	105192	97.7	7	41	21.8 ± 4.9
		ERA5			8.2	33.7	21.1 ± 4.5
	Port Said	Observed	105192	97.8	5.4	40.7	$\mathbf{22.1 \pm 5.4}$
		ERA5			7.6	37.6	21.6 ± 4.8
	El Arish	Observed	105192	95.9	2	45	21.6 ± 6.0
		ERA5			6.9	36.6	21.2 ± 5.0
Relative humidity (RH, %)	Marsa Matrouh	Observed	105192	69.8	4.0	100	70.4 ± 13.0
		ERA5			5.7	100	66.8 ± 17.5
	Abu Qir	Observed	105096	70.1	15	100	$\mathbf{73.2 \pm 9.3}$
		ERA5			18	99.9	71.4 ± 11.1
	Ras El Tin	Observed	105192	75.8	11.0	99.0	68.8 ± 10.4
		ERA5			15.3	100.0	72.3 ± 9.9
	Port Said	Observed	105192	76.7	12.0	100	68.5 ± 11.1
		ERA5			15.7	100	69.6 ± 11.2
	El Arish	Observed	105192	76.4	4	100	70.5 ± 13.1
		ERA5			15.6	100	71.1 ± 11.9
Surface wind speed (WS_{10}, m s^{-1})	Marsa Matrouh	Observed	105192	74.2	0.0	25.4	4.9 ± 3.0
		ERA5			0.0	16.3	4.8 ± 2.1
	Abu Qir	Observed	105096	77.7	0.0	24.3	$\mathbf{6.0 \pm 2.8}$
		ERA5			0.0	16.7	4.5 ± 1.9
	Ras El Tin	Observed	105192	76.9	0.0	24.8	5.4 ± 2.9
		ERA5			0.0	18.6	5.1 ± 2.2
	Port Said	Observed	105192	71.0	0.0	21.6	4.9 ± 2.2
		ERA5			0.0	15.7	4.7 ± 2.0
	El Arish	Observed	105192	65.5	0.0	27.0	4.2 ± 2.4
		ERA5			0.0	17.6	4.2 ± 2.2
Mean sea level pressure (SLP, hPa)	Marsa Matrouh	Observed	105192	97.6	999.5	1034.8	$\mathbf{1015.0 \pm 4.6}$
		ERA5			998.2	1034.9	1014.9 ± 5.0
	Abu Qir	Observed	105096	98.3	992.6	1033.1	1013.8 ± 4.9
		ERA5			990.8	1033.3	1014.2 ± 5.0
	Ras El Tin	Observed	105192	97.8	988.4	1032.3	1013.3 ± 4.8
		ERA5			990.9	1033.5	1014.3 ± 5.0
	Port Said	Observed	105192	99.0	995.9	1033.9	1014.9 ± 4.9
		ERA5			993.6	1032.9	1013.6 ± 5.1
	El Arish	Observed	105192	98.6	996.6	1031.8	1013.7 ± 5.0
		ERA5			996.0	1033.0	1013.5 ± 5.1

quartile values.

Annual trend analysis

C_ERA5 datasets (1979–2020) demonstrate that the annual average of T2m, RH, WS_{10}, and SLP over the studied stations reveals a significant spatial variation, as noticed in Table 5. In the same context, the T2m experienced a positive monotonic trend over the five studied stations. In contrast, the other studied three parameters (RH, WS_{10}, and SLP) over most of the studied stations confirmed a negative monotonic trend. The only exceptions are RH over Marsa Matrouh and WS_{10} over El Arish, which confirm a non-monotonic trend.

In detail, for the period from 1979 to 2020, the warming trend along the study area showed a spatial variation and reached its maximum value along the western side of the study area. Likewise, RH experienced a negative trend along EMC ranging from -0.695% decade^{-1} to non-

significant value where the maximum decrease in RH is expected to be along the western side of the study area. In the same context, WS_{10} presented a negative trend along EMC varied from a non-significant value to -0.053 m s^{-1} decade^{-1} where the maximum decrease is expected to be over the central part of the study area. Finally, SLP experienced a negative trend along the study area and reached its maximum at Marsa Matrouh (-0.127 hPa decade^{-1}) followed by a gently decrease up to El Arish (-0.114 hPa decade^{-1}) as seen in Table 5.

The probability of occurrence

The percentage of occurrences during the hottest hours (mean + 2 × standard deviation) is 1.36% (>30.8°C), 0.44% (>30.6°C), 0.72% (>30.9°C), 1.08% (>31.9°C), and 0.69% (>32.8°C) over Marsa Matrouh, Abu Qir, Ras El-Tin, Port Said, and El Arish respectively as shown in Figure 10A.

The percentage of occurrences during extreme hourly THI events (mean + 2 × standard deviation) is 14.31% (>27.7°C), 17.06% (>28.2°C), 18.12% (>28.3°C), 14.52% (>29.2°C), and 13.57% (>30°C) over Marsa Matrouh, Abu Qir, Ras El-Tin, Port Said, and El Arish respectively as shown in Figure 10B.

The percentage of occurrences during the extreme hourly W_{10} weather events (mean + 2 × standard deviation) is 5.17% (>10.9 m s^{-1}), 4.24% (>11.4 m s^{-1}), 4.05% (>11.2 m s^{-1}), 1.94% (>9.3 m s^{-1}), and 3.76% (>8.8 m s^{-1}), over Marsa Matrouh, Abu Qir, Ras El-Tin, Port Said, and El Arish respectively as shown in Figure 10C.

The percentage of occurrences during the extreme high of hourly SLP (mean + 2 × standard deviation) is 3.19% (>1024.3 hPa), 3.05% (>1023.6 hPa), 2.61% (>1023.2 hPa), 2.87% (>1024.9 hPa), and 2.60% (>1023.7 hPa) over Marsa Matrouh, Abu Qir, Ras El-Tin, Port Said, and El Arish respectively as shown in Figure 10D.

3.3 Statistical downscaling for future projection

This section examines the results of GFDL mini-ensemble mean simulations using various RCPs scenarios for Tas (surface air temperature in the future scenarios), RH, WS_{10}, and SLP.

3.3.1 GFDL model bias correction under the control period, 2007–2020

The GFDL mini-ensemble mean overestimates Tas over Marsa Matrouh, Abu Qir, Port Said, and El Arish by 0.11–0.79°C as seen in Table 6. On the contrary, the GFDL mini-ensemble mean underestimates Tas over Ras El-Tin by 0.94°C. In addition to that, the GFDL mini-ensemble means underestimates RH over Marsa Matrouh, Abu Qir, Ras El-Tin, Port Said, and El Arish by 6.90–23.17%. Similarly, the GFDL mini-ensemble means underestimates WS_{10} over the studied stations by 0.78–2.09 m s^{-1}. In the same context, the GFDL mini-ensemble overestimates SLP over the studied five stations by 4.20–6.73 hPa.

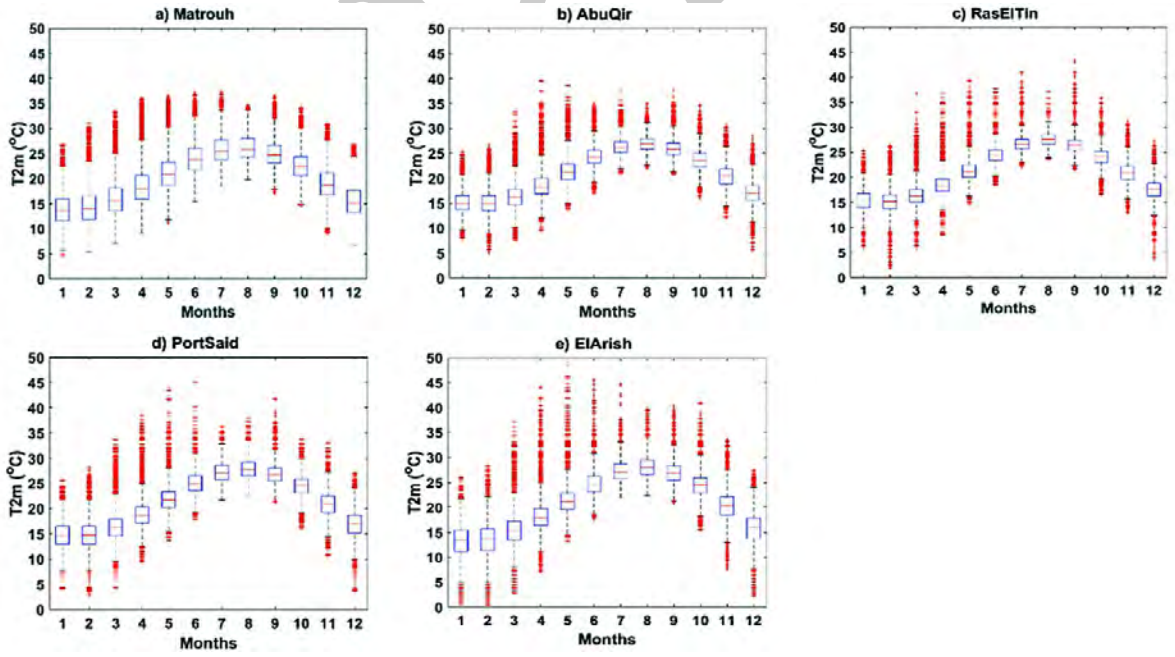

Figure 6. Boxplot analysis for the studied air temperature (T2m) on a monthly basis. The red line in the interior of the box shows the median value. The lower and upper endpoints of the box show the 25th and 75th percentiles. The distance from the 25th to the 75th percentiles is abbreviated by IQR. An arm extending out of each side of the box shows variability outside the upper and lower quartiles as each arm extends no more than 1.5 times the IQR. + sign shows the value of the outlier.

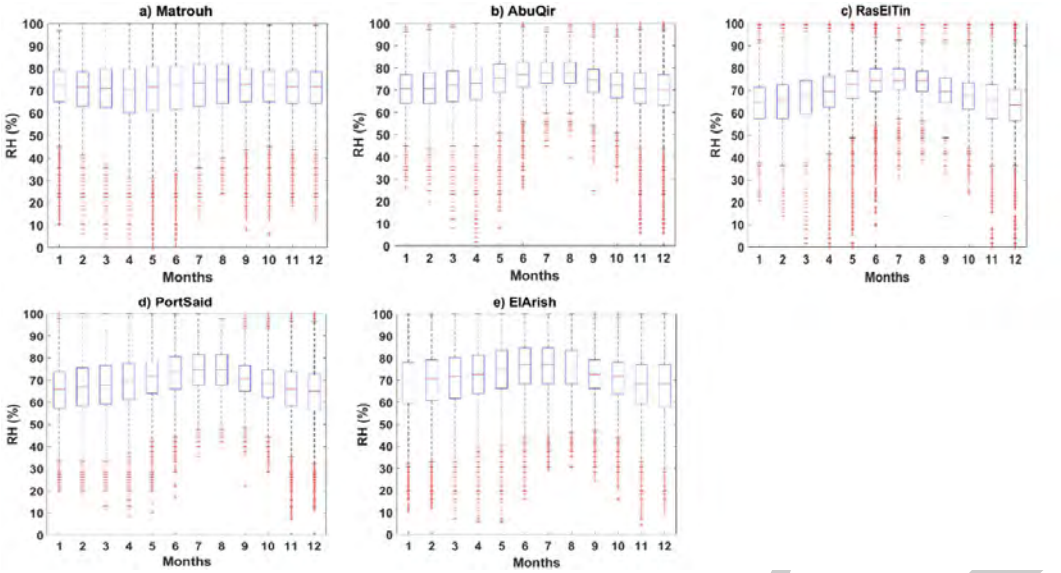

Figure 7. Boxplot analysis for the studied relative humidity (RH) on a monthly basis. Boxplot feature similar to Figure 6.

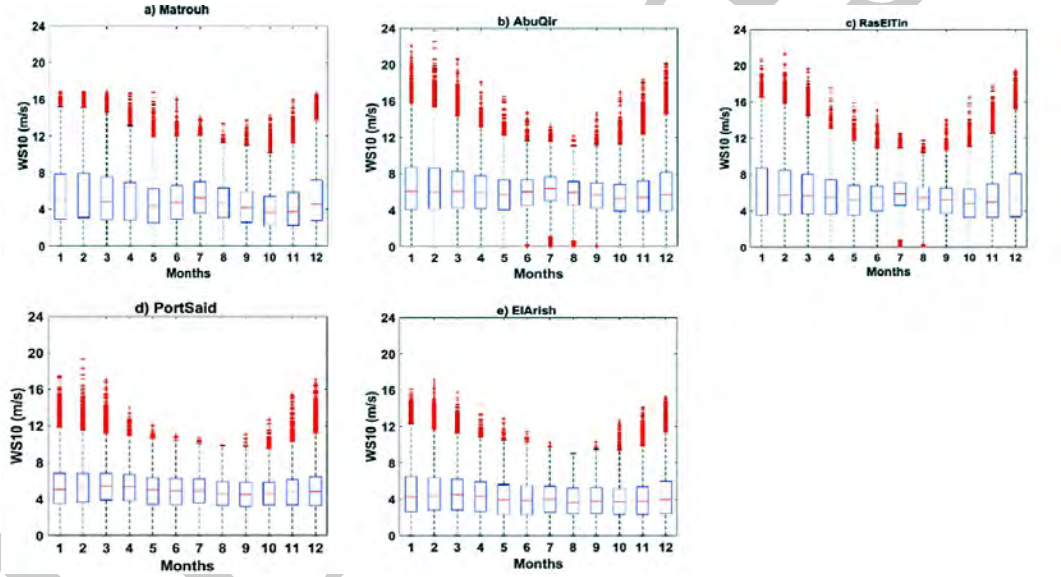

Figure 8. Boxplot analysis for the studied Wind Speed (WS_{10}) on a monthly basis. Boxplot feature similar to Figure 6.

As shown in Annex 3 (Figure A3-2), a simple statistical model was created by comparing the CDF of C_ERA5 with the GFDL mini-ensemble means under a control period (2006–2020) for the various RCPs scenarios in order to overcome the underestimates/overestimates of the GFDL mini-ensemble mean that are incomparable with C_ERA5. The bias adjustment for only RCP2.6 is shown in Annex 3 (Figure A3-2). However, due to the resemblance with RCP2.6 during the control period, the bias correction for RCP4.5, RCP6, and RCP8.5 is not displayed.

3.3.2 Future atmospheric parameters, 2006–2100

Based on the developed statistical model, which was obtained by matching the CDF of the FDL mini-ensemble mean with the CDF of the observation during the control period (2007–2020) for the various RCPs scenarios, the GFDL mini-ensemble mean at each site for the period 2006–2100 was subjected to bias removal to calculate S_D_GFDL mini-ensemble mean simulations (statistically downscaled GFDL mini-ensemble mean). For each site along with the EMC, the S_D_GFDL mini-ensemble means that were calculated were utilized to compute the atmospheric future projections with better accuracy. The 30-

Table 4. The comparison between ERA5 and C_ERA5 in describing the weather characteristics over the studied five stations for the validation period (2019–2020).

Variables	Stations	Validation	R[%]	bias
Surface air temperature (T2M, °C)	Marsa Matrouh	Observed, ERA5	0.964	0.095
		Observed, Corr_ERA5	0.966	0.195
	Abu Qir	Observed, ERA5	0.979	0.346
		Observed, Corr_ERA5	0.979	−0.085
	Ras El Tin	Observed, ERA5	0.975	0.606
		Observed, Corr_ERA5	0.975	−0.08
	Port Said	Observed, ERA5	0.981	0.398
		Observed, Corr_ERA5	0.981	−0.1
	El Arish	Observed, ERA5	0.962	0.239
		Observed, Corr_ERA5	0.963	−0.161
Relative humidity (RH, %)	Marsa Matrouh	Observed, ERA5	0.662	3.272
		Observed, Corr_ERA5	0.667	0.053
	Abu Qir	Observed, ERA5	0.685	3.058
		Observed, Corr_ERA5	0.684	1.36
	Ras El Tin	Observed, ERA5	0.777	−3.889
		Observed, Corr_ERA5	0.778	−0.45
	Port Said	Observed, ERA5	0.768	−0.844
		Observed, Corr_ERA5	0.768	0.267
	El Arish	Observed, ERA5	0.796	−1.783
		Observed, Corr_ERA5	0.796	−1.311
Surface wind speed (WS_{10}, m s^{-1})	Marsa Matrouh	Observed, ERA5	0.749	1.072
		Observed, Corr_ERA5	0.75	0.946
	Abu Qir	Observed, ERA5	0.815	1.87
		Observed, Corr_ERA5	0.816	0.397
	Ras El Tin	Observed, ERA5	0.824	0.999
		Observed, Corr_ERA5	0.825	0.509
	Port Said	Observed, ERA5	0.739	−0.034
		Observed, Corr_ERA5	0.733	−0.193
	El Arish	Observed, ERA5	0.631	−0.768
		Observed, Corr_ERA5	0.632	−0.727
Mean sea level pressure (SLP, hPa)	Marsa Matrouh	Observed, ERA5	0.96	−0.307
		Observed, Corr_ERA5	0.96	−0.404
	Abu Qir	Observed, ERA5	0.985	−0.462
		Observed, Corr_ERA5	0.985	−0.103
	Ras El Tin	Observed, ERA5	0.95	−1.443
		Observed, Corr_ERA5	0.951	−0.505
	Port Said	Observed, ERA5	0.987	1.236
		Observed, Corr_ERA5	0.987	−0.026
	El Arish	Observed, ERA5	0.994	0.237
		Observed, Corr_ERA5	0.994	−0.002

year running average was used to create future projections for the investigated parameters through the four RCP's future scenarios.

S_D_ GFDL mini-ensemble means of projected Tas scenarios of up to 2100 denotes significant warming along the Egyptian Mediterranean coast, notably for the RCP8.5 scenario over El Arish (Figure 11A). The projected warming at the end of the current century (with reference to the 2006–2020 averages value) ranges from 1.43–1.86°C under the RCP8.5 scenario, 0.92–1.17°C under the RCP6.0 scenario, 0.46–0.67°C under the RCP4.5 scenario and 0.08–0.19°C under the RCP2.6 scenario.

Over Marsa Matrouh, S_D_GFDL mini-ensemble means of projected RH scenarios up to 2100 describe a positive trend (non-significant −0.46% $decade^{-1}$). Over Ras El-Tin, S_D_GFDL mini-ensemble means of projected RH scenarios up to 2100 show a significant positive trend through RCP2.6 and RCP4.5 scenario and a non-significant trend through RCP6.0 scenario and a significant negative trend through RCP8.5 scenario. Over Abu Qir, Port Said, and El Arish, S_D_GFDL mini-ensemble means of projected RH scenarios up to 2100 reveal a non-significant trend under

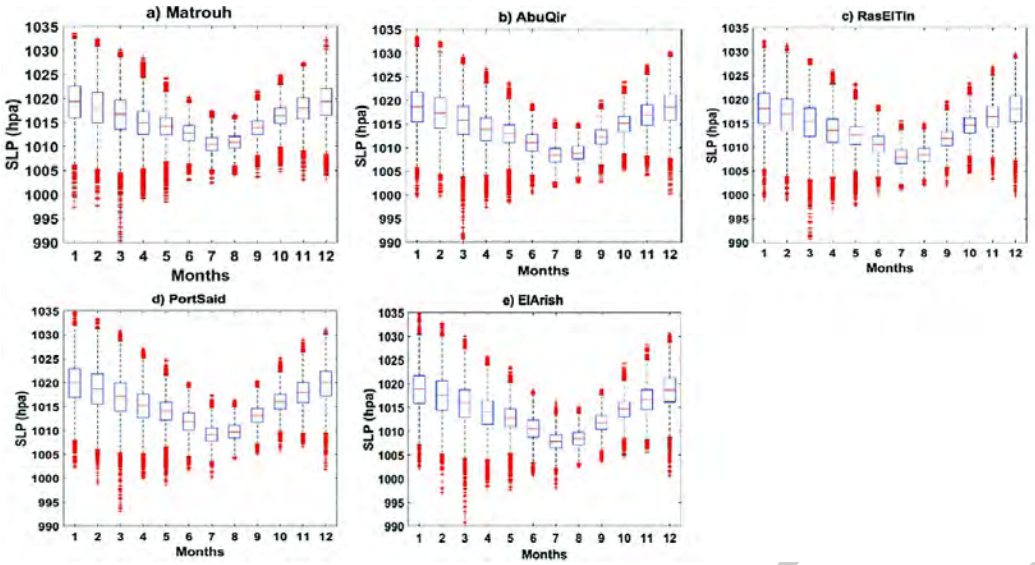

Figure 9. Boxplot analysis for the studied Sea Level Pressure (SLP) on a monthly basis. Boxplot feature similar to Figure 6.

Table 5. Long-term annual mean and trend analyses for corrected ERA5 weather variables over studied stations from 1979 to 2020. The non-parametric (Mann-Kendall test) is used to detect monotonic trends in Corrected ERA5 to examine whether or not C_ERA5 follows a significant (monotonic) trend.

Variables		Annual mean $\pm$ standard deviation of the annual cycle	Trend	Significant (monotonic) trend
Surface air temperature (T2M, °C)	Marsa Matrouh	20.2 ± 5.3	0.309°C decade^{-1}	Yes
	Abu Qir	21.0 ± 4.8	0.405°C decade^{-1}	Yes
	Ras El Tin	21.3 ± 4.8	0.442°C decade^{-1}	Yes
	Port Said	21.3 ± 5.3	0.534°C decade^{-1}	Yes
	El Arish	20.8 ± 6.0	0.566°C decade^{-1}	Yes
Relative humidity (RH, %)	Marsa Matrouh	70.5 ± 12.7	-0.024% decade^{-1}	No
	Abu Qir	73.2 ± 9.7	-0.018% decade^{-1}	Yes
	Ras El Tin	68.8 ± 10.9	-0.060% decade^{-1}	Yes
	Port Said	69.3 ± 11.4	-0.557% decade^{-1}	Yes
	El Arish	71.6 ± 13.0	-0.695% decade^{-1}	Yes
Surface wind speed (WS_{10}, m s^{-1})	Marsa Matrouh	4.9 ± 3.0	-0.023 m s^{-1} decade^{-1}	Yes
	Abu Qir	6.0 ± 2.7	-0.051 m s^{-1} decade^{-1}	Yes
	Ras El Tin	5.6 ± 2.8	-0.053 m s^{-1} decade^{-1}	Yes
	Port Said	4.9 ± 2.2	-0.014 m s^{-1} decade^{-1}	Yes
	El Arish	4.2 ± 2.3	0.002 m s^{-1} decade^{-1}	No
Mean sea level pressure (SLP, hPa)	Marsa Matrouh	1015.3 ± 4.5	-0.127 hPa decade^{-1}	Yes
	Abu Qir	1014.0 ± 4.8	-0.123 hPa decade^{-1}	Yes
	Ras El Tin	1013.6 ± 4.8	-0.126 hPa decade^{-1}	Yes
	Port Said	1015.1 ± 4.9	-0.117 hPa decade^{-1}	Yes
	El Arish	1013.9 ± 4.9	-0.114 hPa decade^{-1}	Yes

RCP2.6 scenario and a significant negative trend under RCP4.5, RCP6.0, and RCP8.5 scenarios (Figure 11B).

S_D_GFDL mini-ensemble means of projected THI scenarios of up to 2100 denote a significant positive trend of risks regarding heat stress along the study area, most markedly for the RCP8.5 scenario over El Arish (Figure 11C). The projected increase in THI at the end of the current century (with reference to 2006–2020 average value) ranges from 1.64–2.09°C under the RCP8.5 scenario, 1.05–1.31°C under the RCP6.0 scenario, 0.57–0.74°C under the RCP4.5 scenario and 0.10–0.22°C under the RCP2.6 scenario (Figure 11C).

S_D_GFDL mini-ensemble means of projected WS_{10} and SLP scenarios up to 2100 confirm a non-significant change up to 2100 (with reference to the 2006–2020 averages value) through the different future RCPs scenarios as seen in Figure 11D and 11E.

Through the study of four future scenarios, the highest projected warming at the end of the current century with reference to the 2006–2020 (hereafter century heating)

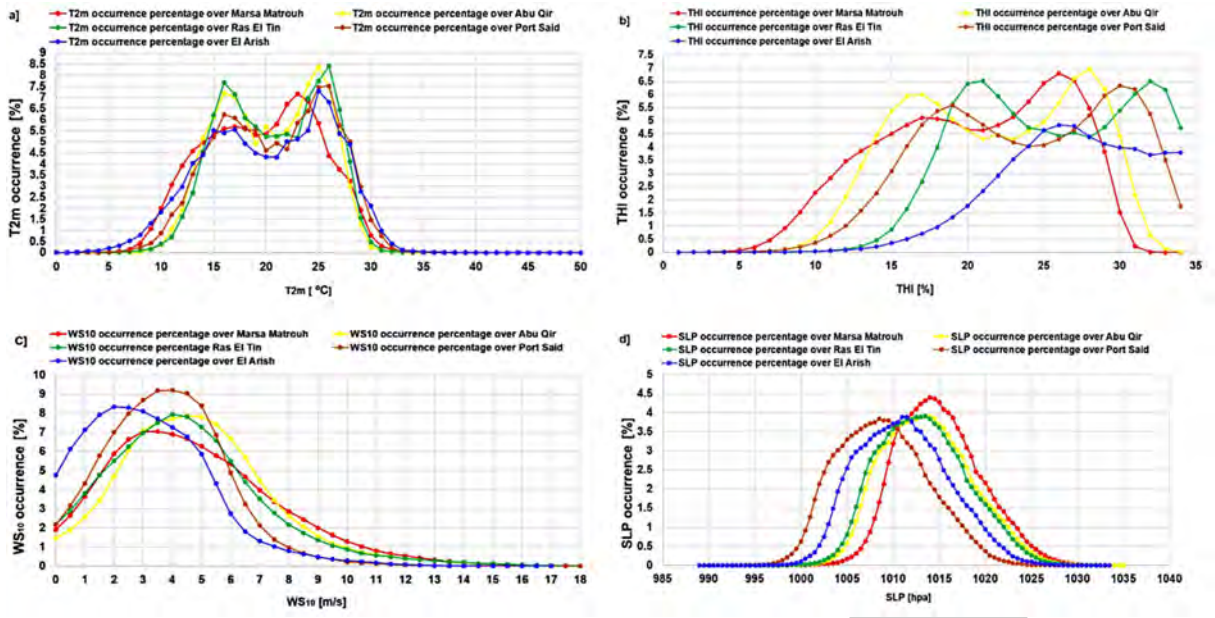

Figure 10. The occurrence percentage of the parameters understudy based on hourly corrected ERA5 data (1979–2020) along the study area.

Table 6. Performance of GFDL mini-ensemble mean in the control period (2007–2020) over Marsa Matrouh, Abu Qir, Ras El Tin, Port Said, and El Arish: only the RCP2.6 scenario is used.

	Annual GFDL mini-ensemble mean – Annual Corrected ERA5			
	Surface air temperature (T2m, °C)	Relative humidity (RH, %)	Surface wind speed (WS_{10}, m s^{-1})	Mean sea level pressure (SLP, hPa)
Marsa Matrouh	0.11	−8.74†	−0.78†	5.66*
Abu Qir	0.73	−23.17†	−2.09†	5.30*
Ras El Tin	−0.94	−6.90†	−1.14†	6.73*
Port Said	0.18	−18.48†	−1.03†	4.20*
El Arish	0.79	−21.20†	−0.96†	4.58*

* Data overestimating performance.
† Data underestimating performance.

occurred over El Arish station. While through scenarios RCP2.6 and RCP4.5, the lowest century heating occurred over Marsa Matrouh station. But through the scenarios RCP6.0 and RCP8.5, the lowest century heating occurred over Abu Qir station. In detail, there is a significant spatial variation in the difference between maximum and minimum century heating (hereafter management uncertainty) along EMC reaching 0.11°C in the RCP2.6 scenario, 0.20°C in the RCP 4.5 scenario, 0.25°C in the RCP6.0 scenario, and 0.43°C in RCP8.5 scenario as seen in Figure 11A.

Similarly, the highest projected RH at the end of the current century with reference to the 2006–2020 (hereafter century RH trend) occurred over Marsa Matrouh station through RCP4.5, RCP6.0, and RCP8.5 scenarios. While through the RCP2.6 scenario, the highest century RH trend occurred over Ras El-Tin. On the contrary, the lowest century RH trend occurred over the El Arish station through RCP4.5, RCP6.0, and RCP8.5 scenarios. While through the RCP2.6 scenario, the lowest century RH trend occurred over Abu Qir station. However, through the RCP2.6 scenario, the lowest century-RH trend occurred over Abu Qir station. In particular, there is a significant spatial variation regarding management uncertainty of RH along EMC reaching 0.09% through scenario RCP2.6, 0.74% through scenario RCP4.5, 0.70% through scenario RCP6, and 0.96% through scenario RCP8.5 as seen in Figure 11B.

In the same context, the highest projected THI at the end of the current century with reference to the 2006–2020 (hereafter century THI trend) occurred over El Arish station. Conversely, the lowest century THI trend occurred over Marsa Matrouh station through RCP2.6 and RCP4.5 scenarios, while through RCP6.0 and RCP8.5 scenarios,

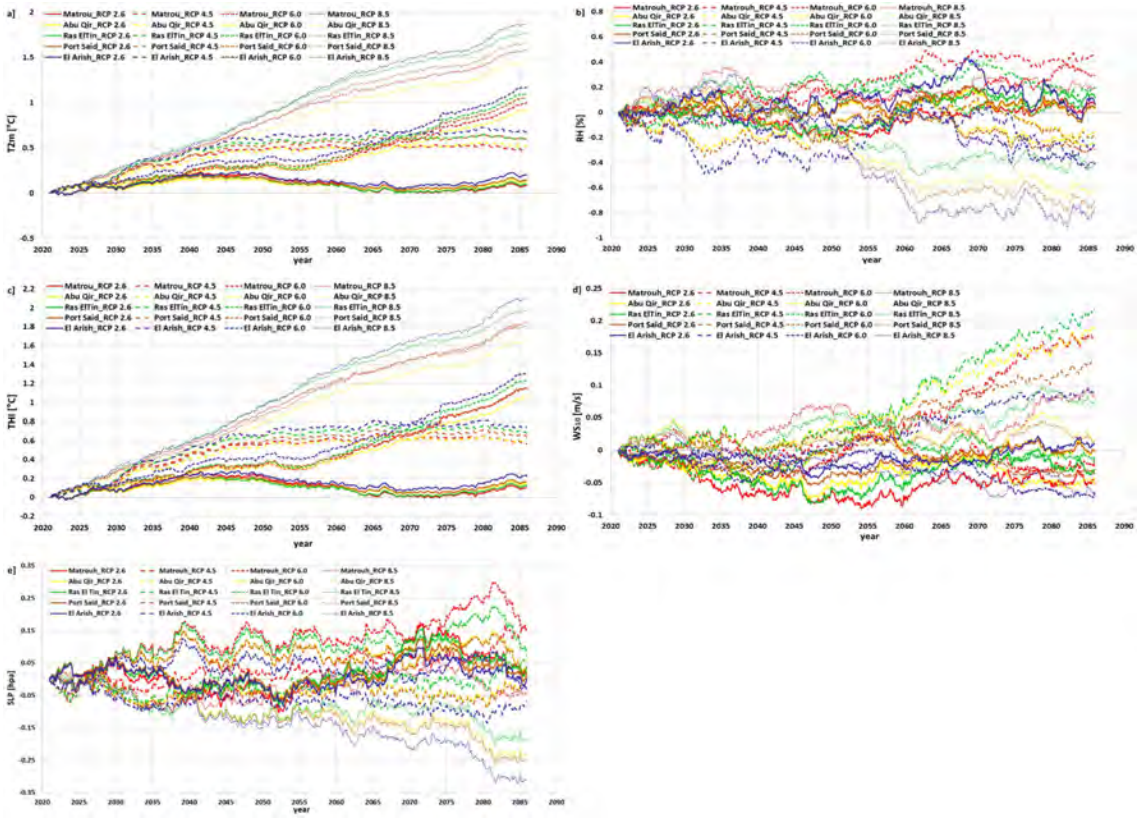

Figure 11. Thirty-year running annual means for (a) Tas (2-m air temperature), (b) RH (relative humidity), (c)THI (temperature humidity index), (d) WS_{10} (surface wind speed), and (e) SLP (mean sea level pressure) anomalies with reference to the 2006–2020 averages for the statically downscaled of the GFDL mini-ensemble mean simulations.

the lowest century THI trend occurred over Abu Qir station. Specifically, there is a significant spatial variation regarding management uncertainty of the THI trend along EMC reaching 0.22°C in scenario RCP2.6, 0.17°C in scenario RCP4.5, 0.26°C in scenario RCP6.0, and 0.45°C in scenario RCP8.5 as seen in Figure 11C.

Finally, the highest projected MSLP at the end of the current century with reference to the 2006–2020, (hereafter century MSLP trend) occurred over Marsa Matrouh station. Conversely, the lowest century MSLP trend occurred over El Arish station. In detail, there is a significant spatial variation regarding management uncertainty of MSLP trend along EMC reaching 0.04 hPa in scenario RCP2.6, 0.25 hPa in scenario RCP4.5, 0.18 hPa in scenario RCP6.0, and 0.26 hPa in scenario RCP8.5 as shown in Figure 11E.

4. Discussion and conclusions

The Egyptian Mediterranean coast is particularly sensitive to climate change for several reasons, including the low-lying delta, saltwater intrusion, high population density, and risks to the economy, agriculture, infrastructure, and ecosystems.

As previously stated, just a few scientific research (Abdelwares et al., 2019; Osman et al., 2021; Elbessa et al., 2021, 2022) have been published regarding the climate along the Egyptian Mediterranean Coast. These few studies focused on dynamical downscaling, highlighting the need for further efforts to enhance our understanding of the current and future climate, especially regarding statistical downscaling. Thus, building an accurate statistical downscaling system to simulate the climate along the Egyptian Mediterranean Coast would be extremely beneficial in providing more trustworthy information to decision-makers.

The current research provided an overview to cover this current gap, based on a few studies on climate projection in Egypt. Moreover, this paper indicates that temperature extremes, together with changes in wind direction, are considered considerable evidence of climate change in Egypt.

We used observation data (2007–2020), and ERA5 reanalysis data (1979–2020) together with GFDL mini-ensemble means (2006–2100) to describe the anatomy of recent surface atmospheric fluctuation along the Egyptian Mediterranean Coast together with building a statistical downscaling model to project the future climatic change. We observed that the maximum air temperature occurred during August. During July, the surface relative humidity reaches its maximum value, and during March, the surface

wind speed reaches its maximum value. The maximum sea level pressure was noticed during January.

Analysis of C_ERA5 (1979–2020) showed that the annual average surface air temperature ranges from 20.2°C over Marsa Matrouh to 21.3°C over Port Said, supporting the previous finding of Shaltout et al. (2013) and El-Geziry et al. (2021). However, Domroes and EL-Tantawi's (2005) results showed lower values than the current analysis simply due to the examination of different time periods. The annual average surface relative humidity ranges from 68.8% over Ras El Tin to 73.2% over Abu Qir, supporting the previous finding of El-Geziry et al. (2021) but showed higher values than Mahfouz et al. (2020) as they analyzed only the period (2007–2018). The annual average wind speed ranges from 4.2 m s^{-1} over El Arish to 6.0 m s^{-1} over Abu Qir, giving higher values than the previous finding of Essa and Mubarak (2006). This disagreement is due to the only five years analysis (2000–2004) by Essa and Mubarak (2006). The annual average sea level pressure ranges from 1013.6 hPa over Ras El Tin to 1015.3 hPa over Marsa Matrouh, supporting the previous results of Shaltout et al. (2013) and Mahfouz et al. (2020).

Depending on C_ERA5 (1979–2020), the historical maximum record of surface air temperature, wind speed, sea level pressure, and temperature humidity index were 49.12°C, 23.75 m s^{-1}, 1034.92 hPa, and 32.92°C respectively. In the same context, the historical minimum record of air temperature, sea level pressure, and temperature humidity index were −2.21°C, 989.83 hPa, and −8°C, respectively.

In general, the prevailing wind along the Egyptian Mediterranean coast fluctuates between North to Northwest, with significant monthly variation between the Southern, Western, Northern, and Northwesterly. The new inference in this paper about the southern wind from 00.00 to 08.00 at El Arish will give new directions to the coming research to understand this phenomenon and its effect on ocean eddies, currents, and sea waves.

The ERA5 lower estimate T2m, RH, WS_{10}, and SLP along the study area by 0.39°C, 0.04%, 0.42 m s^{-1}, and 0.04 hPa, respectively. Moreover, ERA5 closely describes the atmospheric parameters along EMC with a significant correlation, reaching its maximum value of 98.3% (n = 613422) for SLP and reaching its minimum value of 73.1% (n = 613423) for WS_{10}. Generally, ERA5 reanalysis data simulated efficiently the studied atmospheric parameter over all stations. Moreover, the C_ERA5 dataset indicates that the study area experiences significant warming trends together with a monotonic decrease in RH, WS_{10}, and SLP. From another perspective, the principal component analysis proves that the pattern linking the studied four parameters differs from station to station.

Generally, the present study verified that the ERA5 reanalyzed data following bias correction are extremely beneficial for climate research over EMC, providing high-resolution, long-term, and consistent climate data necessary for studies, model validation, adaptation planning, and climate change analysis.

In the control period (2007–2020), the GFDL mini-ensemble mean overestimates (underestimates) Tas and SLP (RH and WS_{10}). This indicates the importance of using bias removal techniques (CDF) to correct the GFDL mini-ensemble mean so that it is valid for the studied area.

Further CDF techniques were used to statistically downscale GFDL mini-ensemble mean simulations along the Egyptian Mediterranean Coast. We predict that the study area will experience significant warming and increases in risks regarding heat stress. In the same context, RH's future scenarios show a wide range of negative to positive trends. Projected WS_{10} and SLP will experience non-significant changes up to 2100. This projected future warming supports the previous findings of Lelieveld et al. (2016), Bucchignani et al. (2018), and Elbessa et al. (2022). Moreover, the non-significant change in projected future SLP is slightly different from the previous findings of Shaltout et al. (2013), who suggested a slight decrease in future SLP through different SRES scenarios.

Generally, the future warming uncertainty is 1.8°C. 87% of this uncertainty is related to scenario design, while 13% of this uncertainty is related to regional variation. This shows that management actions should prioritize reducing emissions. For future RH, the uncertainty is 1.2%; 49% of it is associated with regional variation, and 43% is associated with scenario design. This demonstrates that any future sustainability plan should take regional variance into account. For the future THI, the uncertainty is 2°C; 87% of it is associated with the scenario design, and 13% is associated with regional variation. We suggest that the risks regarding heat stress along the study area are projected to be over 32°C to trigger sunstroke and heat exhaustion.

Under a high-emissions scenario, the IPCC (2022) finds that the world may warm by 4.4°C by 2100. Alpert et al. (2008) showed that the eastern Mediterranean may warm by 4°C by the end of the current century. However, Shaltout et al. (2013) confirmed that the Egyptian Mediterranean Coast may warm by 2.6°C by 2100. The current study confirmed that the EMC will experience significant warming up to 1.8°C by the end of the current century, roughly 0.4 times the global response. Moreover, the current research showed a lower estimate of the highest possible temperature at the end of the current century by about 0.69% with respect to Shaltout et al. (2013). This disagreement can be explained by the methods Shaltout et al. (2013) used, which were based on the use of the global climate model without applying any downscaling techniques. Changes in air circulation, particularly during the winter when the Siberian winter is high, affect the study area by lowering the temperature, which can explain this moderate warming along the EMC.

Based on the detailed analysis of climate projections across the studied RCPs future scenarios and various climate parameters (Tas, RH, THI, WS_{10}, and SLP) over five stations along EMC. There is a significant spatial variation in climate change impacts along EMC. All the studied stations experience varying levels of warming and changes in RH, THI, and SLP trends depending on the emission scenarios considered. In detail, the choice of emission scenario (RCP2.6 to RCP8.5) profoundly influences the magnitude of climate change impacts. Higher emission scenarios (RCP8.5) generally project more severe changes compared to lower emission scenarios (RCP2.6). Specifically, each of the studied stations exhibits unique characteristics in response to climate change. For example, El Arish station consistently shows higher warming trends, while Marsa Matrouh often experiences higher RH and THI trends.

In conclusion, these findings have significant implications for regional climate adaptation and mitigation strategies along EMC. They highlight the need for localized assessments and adaptive measures suitable to specific climate risks faced by different regions and communities.

Van Vuuren et al. (2011) stated that there is no consistent set of socioeconomic assumptions in any of the considered four RCPs scenarios. Thus, in our future work, we will employ our statistical downscaling using The Shared Socioeconomic Pathways (SSPs) scenarios (IPCC, 2023). Moreover, we confirm in our current work that we will no longer utilize the RCP8.5 scenario as the most likely one, and that it should only be used to study a highly unlikely but unlikely future. For example, the annual T2m mean measurements of 20.6°C, 21.51°C, 21.8°C, 22.1°C and 21.6°C recorded over Marsa Matrouh, Ras El-Tin, Abu Qir, Port Said, and El Arish during (2007–2020), respectively. It's expected to rise to 21.6°C, 22.4°C, 22.9°C, 23.2°C and 22.8°C, respectively through RCP6.0 (probable) scenario by 2100. This expected warming may rise to 23.2°C, 23.9°C, 24.7°C, 24.8°C and 24.6°C, respectively, through the RCP8.5 (improbable, high-risk future) scenario by 2100.

The previous research stated that this region is drought-prone, and climate change may exacerbate this problem. Thus, studying the current and future projections of precipitation merits our consideration and will be studied in our future work due to the singularity. The used atmospheric data did not contain precipitation thus we plan to use TRMM and GES DISC databases to describe the current precipitation variability.

The present work is considered the first attempt to statistically downscale the future climate along the Egyptian Mediterranean Coast. The current results, together with previously dynamical downscaling results (Elbessa et al., 2022), enrich the uncertainty analysis of the future climate. Moreover, the authors are willing to expand the studied statistical tool to cover the Egyptian Red Sea coast. Finally, the current research sheds light on the importance of studying the effect of climate change on several concerns as a result of future climate change, including issues with its water resources, agriculture, health, economy, biodiversity, and social stability. Coordinated efforts in adaptation, mitigation, policy-making, and international collaboration will be needed to address these issues.

We are now able to better understand the science behind climate change, better analyze the current atmospheric characteristics, and better model the future to support addressing the causes and consequences of climate change.

Declaration of competing interest

The authors declare that they have no known competing financial interests or personal relationships that could have appeared to influence the work reported in this paper.

Acknowledgement

The authors would like to express their sincere thanks to the project "Downscaling atmospheric components over Egypt under different future climate change scenarios (2065–2100)" that is funded by the Academy for Scientific Research and Technology for providing a supercomputer for the current research analysis.

Supplementary materials

Please follow this link to see the supplementary material associated with this article.

References

Abdelwares, M., Lelieveld, J., Hadjinicolaou, P., Zittis, G., Wagdy, A., Haggag, M., 2019. *Evaluation of a regional climate model for the eastern Nile basin: Terrestrial and atmospheric water balance*. Atmosphere 10 (12). https://doi.org/10.3390/ATMOS10120736

Agrawala, S., Moehner, A., Gagnon-Lebrun, F., Van Aalst, M., Smith, J., Hagenstad, M., El Raey, M., Conway, D., 2004. *Development and Climate Change in Egypt. Focus on Coastal Resources and the Nile*. International Nuclear Information System (INIS), 36 (1).

Ahmad, I., Tang, D., Wang, T., Wang, M., Wagan, B., 2015. *Precipitation trends over time using Mann-Kendall and Spearman's Rho tests in the Swat River Basin, Pakistan*. Adv. Meteorol. 431860, 15 pp. https://doi.org/10.1155/2015/431860

Alcamo, J., Moreno, J.M., Novaky, B., Bindi, M., Corobov, R., Devoy, R.J.N, Giannakopoulos, C., Martin, E., Olesen, J.E., Shvidenko, A., 2007. *Europe*. [In:] *Climate Change 2007: Impacts, adaptation, and vulnerability. Contribution by Working Group II to the Fourth Assessment Report of the Intergovernmental Panel on Climate Change*, Parry, M.L., Canziani, O.F., Palutikof, J.P., van der Linden, P.J., Hanson, C.E. (Eds.), Cambridge University Press, Cambridge, UK, 541–580.

Alduchov, O.A., Eskridge, R.E., 1996. *Improved Magnus Form Approximation of Saturation Vapor Pressure*. J. Appl. Meteorol. 35(4), 601–609. https://doi.org/10.2172/548871

Alpert, P., Krichak, S.O., Shafir, H., Haim, D., Osetinsky, I., 2008. *Climatic trends in extremes employing regional modeling and statistical interpretation over the E. Mediterranean*. Global and Planetary Change 63(2–3), 163–170. https://doi.org/10.1016/j.gloplacha.2008.03.003

Anagnostou, E.N., Negri, A.J., Adler, R.F., 1999. *Statistical Adjustment of Satellite Microwave Monthly Rainfall Estimates over Amazonia*. J. Appl. Meteorol. 38, 1590–1598.

Bawadekji, A., Tonbol, K., Ghazouani, N., Becheikh, N., Shaltout, M., 2022. *Recent atmospheric changes and future projections along the Saudi Arabian Red Sea Coast*. Sci. Rep. 12(1). https://doi.org/10.1038/s41598-021-04200-z

Bucchignani, E., Mercogliano, P., Panitz, H.J., Montesarchio, M., 2018. *Climate change projections for the Middle East-North Africa domain with COSMO-CLM at different spatial resolutions*. Adv. Clim. Change Res. 9(1), 66–80. https://doi.org/10.1016/j.accre.2018.01.004

Copernicus Climate Change Service (C3S), 2017. *ERA5: Fifth generation of ECMWF atmospheric reanalysis of the global climate*. Copernicus Climate Change Service Climate Data Store (CDS), 23 July 2020. https://cds.climate.copernicus.eu/cdsapp#!/home

De Vries, A.J., Tyrlis, E., Edry, D., Krichak, S.O., Steil, B., Lelieveld, J., 2013. *Extreme precipitation events in the Middle East: Dynamics of the Active Red Sea Trough*. J. Geophys. Res. 118(13), 7087–7108. https://doi.org/10.1002/jgrd.50569

Domroes, M., El-Tantawi, A., 2005. *Recent temporal and spatial temperature changes in Egypt*. Int. J. Climatol. 25(1), 51–63. https://doi.org/10.1002/joc.1114

Dunne, J.P., John, J.G., Adcroft, A.J., Griffies, S.M., Hallberg, R.W., Shevliakova, E., Stouffer, R.J., Cooke, W., Dunne, K.A., Harrison, M.J., Krasting, J.P., Malyshev, S.L., Milly, P.C.D., Phillipps, P.J., Sentman, L.T., Samuels, B.L., Spelman, M.J., Winton, M., Wittenberg, A.T., Zadeh, N., 2012. *GFDL's ESM2 global coupled climate-carbon earth system models. Part I: Physical formulation and baseline simulation characteristics*. J. Climate 25(19), 6646–6665. https://doi.org/10.1175/JCLI-D-11-00560.1

Dunne, J.P., John, J.G., Shevliakova, S., Stouffer, R.J., Krasting, J.P., Malyshev, S.L., Milly, P.C.D., Sentman, L.T., Adcroft, A.J., Cooke, W., Dunne, K.A., Griffies, S.M., Hallberg, R.W., Harrison, M.J., Levy, H., Wittenberg, A.T., Phillips, P.J., Zadeh, N., 2013. *GFDL's ESM2 global coupled climate-carbon earth system models. Part II: Carbon system formulation and baseline simulation characteristics*. J. Climate 26(7), 2247–2267. https://doi.org/10.1175/JCLI-D-12-00150.1

Egyptian Naval Forces, 1962. *Theoretical of meteorology*, Egyptian Navy Publication, Educational Authority, 125 pp.

Elbessa, M., Abdelrahman, S.M., Tonbol, K., Shaltout, M., 2021. *Dynamical downscaling of surface air temperature and wind field variabilities over the southeastern levantine basin and Mediterranean Sea*. Climate 9(1). https://doi.org/10.3390/cli9100150

Elbessa, M., Abdelrahman, S.M., Tonbol, K., Shaltout, M., 2022. *Modeling the future scenarios for surface temperature and wind regime over the South-Eastern Levantine Basin, Egypt*. Egyptian J. Aquatic Biol. Fish. 26(3), 541–564. https://doi.org/10.21608/ejabf.2022.244114

El-Geziry, T.M., Elbessa, M., Tonbol, K.M., 2021. *Climatology of Sea–Land Breezes Along the Southern Coast of the Levantine Basin*. Pure Appl. Geophys. 178(5), 1927–1941. https://doi.org/10.1007/s00024-021-02726-x

Elsharkawy, M.S., El-Geziry, T.M., El-Din, S.H.S., 2016. *General Characteristics of Surface Waves off Port Said, Egypt*. IOSR J. Environ. Sci. Toxicol. Food Tech. 10(08).

Essa, K.S.M., Mubarak, F., 2006. *Survey and Assessment of Wind-Speed and Wind-power in Egypt, Including Air Density Variation*. Wind Engineering 30(2), 95–106. https://doi.org/10.1260/030952406778055081109-115

Griffies, S.M., Winton, M., Donner, L.J., Horowitz, L.W., Downes, S.M., Farneti, R., Gnanadesikan, A., Hurlin, W.J., Lee, H.C., Liang, Z., Palter, J.B., Samuels, B.L., Wittenberg, A.T., Wyman, B.L., Yin, J., Zadeh, N., 2011. *The GFDL CM3 coupled climate model: Characteristics of ocean and sea ice simulations*. J. Climate, 24(13), 3520–3544. https://doi.org/10.1175/2011JCLI3964.1

Haggag, M., El-Badry, H., 2013. *Mesoscale Numerical Study of Quasi-Stationary Convective System over Jeddah in November 2009*. Atmos. Climate Sci. 03(01), 73–86. https://doi.org/10.4236/acs.2013.31010

Hamed, A.A., 1979. *Atmospheric Circulation Features Over the Southeastern Part of the Mediterranean Sea in Relation with Weather Conditions and Wind Waves at Alexandria*. M.Sc. Thesis, Alexandria University, Egypt.

Hamed, A.A., 1983. *Atmospheric Circulation over the Southeastern Part of the Mediterranean Sea in Relation with Weather Conditions and Wind Waves Along the Egyptian Coast*. Ph.D. Thesis, Alexandria University, Egypt.

Hersbach, H., Bell, B., Berrisford, P., Biavati, G., Horányi, A., Muñoz Sabater, J., Nicolas, J., Peubey, C., Radu, R., Rozum, I., Schepers, D., Simmons, A., Soci, C., Dee, D., Thépaut, J-N., 2020. *ERA5 hourly data on single levels from 1979 to the present*. Copernicus Climate Change Service (C3S) Climate Data Store (CDS) (accessed on 09-01-2021). https://doi.org/10.24381/CDs.adbb2d47.

Hausfather, Z., Peters, G., 2020. *Emissions – the "business as usual" story is misleading*. Nature 577 (2020), 618–620. https://doi.org/10.1038/d41586-020-00177-3

IPCC, 2014. *Climate change 2014: impacts, adaptation, and vulnerability*. Working Group II contribution to the fifth assessment report of the Intergovernmental Panel on Climate Change, Pt. A, Cambridge University Press, New York.

IPCC, 2019. *Special Report – Global Warming of 1.5°C*. Report of the Intergovernmental Panel on Global Warming. https://www.ipcc.ch/sr15/

IPCC, 2022. *Strengthening and Implementing the Global Response*. [In:] *Global Warming of 1.5°C: IPCC Special Report on Impacts of Global Warming of 1.5°C above Pre-Industrial Levels in Context of Strengthening Response to Climate Change, Sustainable Development, and Efforts to Eradicate Poverty*. Cambridge University Press, 313–444. https://doi.org/10.1017/9781009157940.006

IPCC, 2023. *Climate Change 2023: Synthesis Report*. Contribution of Working Groups I, II and III to the Sixth Assessment Report of the Intergovernmental Panel on Climate Change Geneva, Switzerland, 35–115. https://doi.org/10.59327/IPCC/AR6-9789291691647

Kautz, L.A., Martius, O., Pfahl, S., Pinto, J.G., Ramos, A.M., Sousa, P.M., Woollings, T., 2022. *Atmospheric blocking and weather extremes over the Euro-Atlantic sector – A review*. Weather and Clim. Dynam. 3(1), 305–336. https://doi.org/10.5194/wcd-3-305-2022

Kendall M.G., 1975. *Rank Correlation Methods*. 4th edn., Charles Griffin, London, UK.

Krichak, S.O., Alpert, P., Bassat, K., Kunin, P., 2007. *The surface climatology of the eastern Mediterranean region obtained in a three-member ensemble climate change simulation experiment*. Adv. Geosci. 12, 67–80. https://doi.org/10.5194/adgeo-12-67-2007

Lelieveld, J., Proestos, Y., Hadjinicolaou, P., Tanarhte, M., Tyrlis, E., Zittis, G., 2016. *Strongly increasing heat extremes in the Middle East and North Africa (MENA) in the 21st century*. Climatic Change 137(1–2), 245–260. https://doi.org/10.1007/s10584-016-1665-6

Liljegren, J.C., Carhart, R.A., Lawday, P., Tschopp, S., Sharp, R., 2008. *Modeling the wet bulb globe temperature using standard meteorological measurements*. J. Occup. Environ. Hyg. 5(10), 645–655. https://doi.org/10.1080/15459620802310770

Lionello, P., Bhend, J., Buzzi, A., Della-Marta, P.M., Krichak, S.O., Jansà, A., Maheras, P., Sanna, A., Trigo, I.F., Trigo, R., 2006. *Chapter 6 Cyclones in the Mediterranean region: Climatology and effects on the environment*. [In:] *Developments in Earth and Environmental Sciences*, Vol. 4, 325–372. https://doi.org/10.1016/S1571-9197(06)80009-1

Mahfouz, B.M.B., Osman, A.G.M., Saber, S.A., Kanhalaf-Allah, H.M.M., 2020. *Assessment of weather and climate variability over the western harbor of Alexandria, Egypt*. Egyptian J. Aquatic Biol. Fish. 24(5), 323–339. https://doi.org/10.21608/EJABF.2020.105861

Mann H.B., 1945. *Non-parametric test against trend*, Econometrica 13, 245–259. https://doi.org/10.2307/1907187.

Meligy, M.M., 2000. *Wave and Surge Forecasting Along the Egyptian Coast of the Mediterranean*. M.Sc. Thesis, Arab Academy for Science and Technology and Maritime Transport, Alexandria Governorate, Egypt.

Moss, R.H., Edmonds, J.A., Hibbard, K.A., Manning, M.R., Rose, S.K., Van Vuuren, D.P., Carter, T.R., Emori, S., Kainuma, M., Kram, T., Meehl, G.A., 2010. *The next generation of scenarios for climate change research and assessment*. Nature, 463(7282), 747–756.

Nastos, P.T., Zerefos, C.S., 2009. *Spatial and temporal variability of consecutive dry and wet days in Greece*. Atmos. Res. 94(4), 616–628. https://doi.org/10.1016/j.atmosres.2009.03.009

Osman, M., Zittis, G., Haggag, M., Abdeldayem, A.W., Lelieveld, J., 2021. *Optimizing Regional Climate Model Output for Hydro-Climate Applications in the Eastern Nile Basin*. Earth Sys. Environ. 5(2), 185–200. https://doi.org/10.1007/s41748-021-00222-9

Reichle, R.H., Koster, R.D., 2004. *Bias reduction in short records of satellite soil moisture*. Geophys. Res. Lett. 31(19). https://doi.org/10.1029/2004GL020938

Riahi, K., Rao, S., Krey, V., Cho, C., Chirkov, V., Fischer, G., Kindermann, G., Nakicenovic, N., Rafaj, P., 2011. *RCP 8.5—A scenario of comparatively high greenhouse gas emissions*. Climatic Change 109, 33–57.

Saaroni, H., Bitan, A., Alpert, P., Ziv, B., 1996. *Continental polar outbreaks into the Levant and eastern Mediterranean*. Int. J. Climatol. 16, 1175–1191. https://doi.org/10.1002/(SICI)1097-0088(199610)16:10<1175:AID-JOC79>3.0.CO;2

Saaroni, H., Ziv, B., Bitan, A., Alpert, P., 1998. *Easterly wind storms over Israel*. Theor. Appl. Climatol. 59(1–2), 61–77. https:/doi.org/10.1007/s007040050013

Sabra, F.A., 1979. *Wind, current and sea level variations over the continental shelf Alexandria coast*. M.Sc. Thesis, Alexandria University, Egypt, 52–60.

Sallam, G.A.H., Elsayed, E.A., 2015. *Estimating the impact of air temperature and relative humidity change on the water quality of Lake Manzala, Egypt*. J. Nat. Resour. Dev. 5., 76–87. https://doi.org/10.5027/jnrd.v5i0.11

Shaltout, M., El Gindy, A., Omstedt, A., 2013. *Recent climate trends and future scenarios in the Egyptian Mediterranean coast based on six global climate models*. Geofizika J. 30(1), 19–41.

Tuel, A., Eltahir, E.A.B., 2020. *Why Is the Mediterranean a Climate Change Hot Spot?* J. Climate, 33(14), 5829-5843. https://doi.org/10.1175/JCLI-D-19-0910.1

Tonbol, K.M., El-Geziry, T.M. and Elbessa, M., 2018. *Evaluation of Changes and Trends of Air Temperature within the Southern Levantine Basin*. Weather, 73(2), 60–66. https://doi.org/10.1002/wea.3186

UNESCO, 1979. *Map of the world distribution of arid regions (Explanatory note)*. MAB Tech. Notes 7, Unesco, Paris, 54 pp.

Wang, F., Shao, W., Yu, H., Kan, G., He, X., Zhang, D., Ren, M., Wang, G., 2020. *Re-evaluation of the Power of the Mann-Kendall Test for Detecting Monotonic Trends in Hydrometeorological Time Series*. Front. Earth Sci. 8. https://doi.org/10.3389/feart.2020.00014

Van Vuuren, D.P., Edmonds, J., Kainuma, M., Riahi, K., Thomson, A., Hibbard, K., Hurtt, G.C., Kram, T., Krey, V., Lamarque, J.F., Masui, T., 2011. *The representative concentration pathways: an overview*. Climatic Change, 109, 5–31.

Vigaud, N., Vrac, M., Caballero, Y., 2013, *Probabilistic downscaling of GCM scenarios over southern India*. Int. J. Climatol. 33, 1248–1263. https://doi.org/10.1002/joc.3509

Vaittinada Ayar, P., Vrac, M., Mailhot, A., 2021. *Ensemble bias correction of climate simulations: preserving internal variability*. Sci. Rep. 11, 3098. https://doi.org/10.1038/s41598-021-82715-1

Williamson, D.F., Parker, R.A., Kendrick, J.S., 1989. *The box plot: A simple visual method to interpret data*. Ann. Intern. Med. 110(11), 916–921. https://doi.org/10.1059/0003-4819-110-11-916

Wood, A.W., Maurer, E.P., Kumar, A., Lettenmaier, D.P., 2002. *Long-range experimental hydrologic forecasting for the eastern United States*. J. Geophys. Res. 107(20), ACL 6-1–ACL 6-15. https://doi.org/10.1029/2001JD000659

Yadav, R.K., 2021. *Relationship between Azores High and Indian summer monsoon*. NPJ Clim. Atmos. Sci. 4(1). https://doi.org/10.1038/s41612-021-00180-z

Zecchetto, S., De Biasio, F., 2007. *Sea surface winds over the Mediterranean basin from satellite data (2000–04): Meso- and local-scale features on annual and seasonal time scales*. J. Appl. Meteorol. Clim. 46(6), 814–827. https://doi.org/10.1175/JAM2498.1

Zerefos, C., Repapis, C., Giannakopoulos, C., Kapsomenakis, J., Papanikolaou, D., Papanikolaou, M., Poulos, S., Vrekoussis, M., Philandras, C., Tselioudis, G., Gerasopoulos, E., Douvis, K., Diakakis, M., Nastos, P., Hadjinicolaou, P., Xoplaki, E., Luterbacher, J., Zanis, P., Tzedakis, C., Repapis, K., 2011. *The climate of the Eastern Mediterranean and Greece: past, present, and future*. [In:] *The Environmental, Economic and Social Impacts of Climate Change in Greece*. Bank of Greece, Athens, 1–126.